

CLEARED FOR PUBLIC RELEASE

PL/PA 16 DEC 96

Sensor and Simulation Notes

Note 172

March 1973

Pulse Propagation in a Ground Transmission
Line EMP Simulator

by

W. E. Page
Air Force Weapons Laboratory

T. L. Brown
The Dikewood Corporation

Abstract

The propagation of a guided pulse in a configuration approximating an EMP simulator has been analyzed. The results of a time domain finite difference calculation are presented and compared with time waveforms obtained from a waveguide approximation. Convergence of the results for lower frequencies is shown.

PL 96-11975

Acknowledgement

Patient encouragement in completing the comparisons has been provided by Carl Baum and is gratefully acknowledged.

I. Introduction

A finite difference technique for analyzing the early time propagation of an EM pulse guided over the ground in a manner approximating an EMP simulator has been developed by Page¹. This method consisted of a time domain finite difference using a dynamic computational mesh. A parametric set of calculations was also done.

A method of analysis for this problem has been described by Baum^{2, 3}. This method, which is based on a waveguide approximation, has subsequently been extended to allow the frequency domain calculation of fields above and below the ground. These results were used to obtain time domain waveforms by means of a numerical calculation of the inverse fourier transform.

The results of the finite difference calculation are presented here along with comparable calculations using the waveguide approximation. These results are given in the form of time domain waveforms which have been carried far enough in time to illustrate the convergence of the waveguide approximation to the finite difference calculations at lower frequencies.

II. Finite Difference Calculation

The geometry of the finite difference calculation is given in figure 1-A. The configuration is assumed to be infinitely wide (in the z direction) and the fields are taken to vary in the two spatial dimensions x and y. This geometry approximates an actual ground transmission line simulator for points near the centerline where fringing effects are negligible.

It is assumed that a plane electromagnetic wave is propagating in the positive x direction. This wave has only a positive y component of the E-field (E_{y_0}) and a corresponding z component of the B-field (B_{z_0}). All the computed fields are then normalized to the amplitude of this initial plane wave, i. e.:

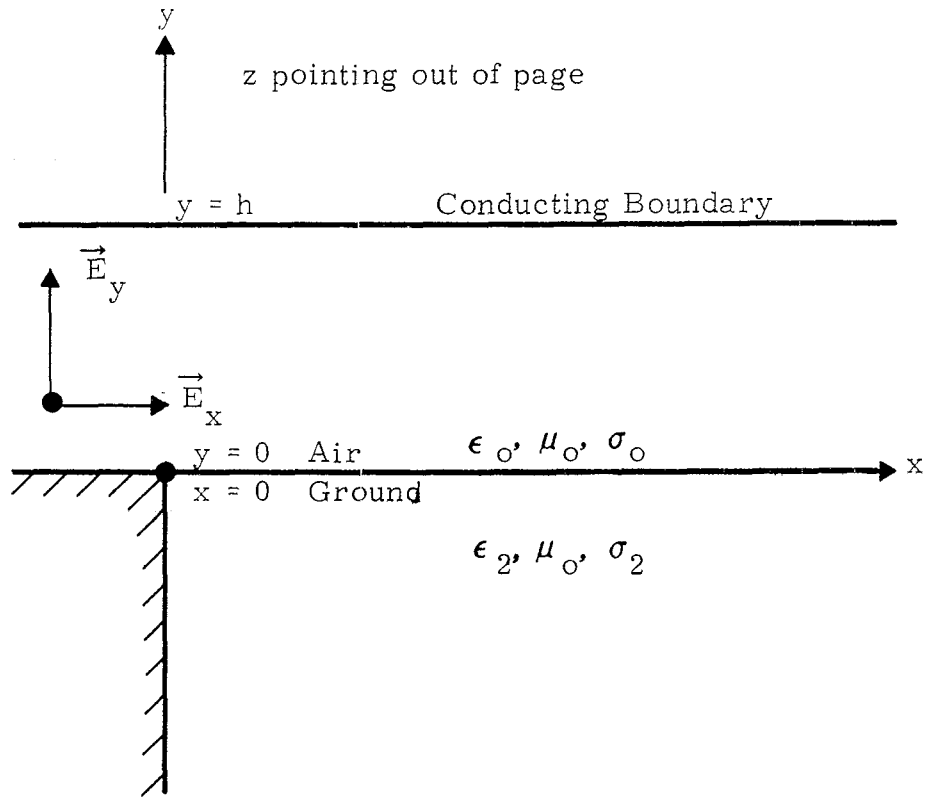
$$B = \frac{B_{z_c}}{B_{z_0}}, \quad E_y = \frac{E_{y_c}}{E_{y_0}} \quad \text{and} \quad E_x = \frac{E_{x_c}}{E_{x_0}} \quad (1)$$

The pulse propagates as a plane wave until the air-ground interface is reached. Diffraction from the ground then establishes an x component of the electric field. The effect of this refraction continues to alter the assumed incident plane waveform as the pulse propagates across the simulator. The finite difference calculation determines the x and y components of the E-field and the z component of the B-field as a function of time throughout the configuration.

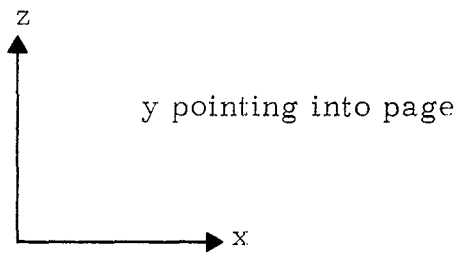
In the wave equation

$$\nabla^2 \phi - \mu \epsilon \ddot{\phi} - \mu \sigma \dot{\phi} = 0 \quad (2A)$$

a fundamental length h (the height of the conducting boundary above the ground as shown in Figure 1) and a corresponding fundamental time $T = h/c$ are introduced obtaining new non-dimensional coordinates



A. Cartesian Coordinate Geometry of Finite Difference Model.



B. Cartesian Coordinate of Waveguide Model.

Figure 1. Surface Transmission Line Simulator.

$$X' = \frac{x}{h} \quad Y' = \frac{y}{h} \quad T' = \frac{t}{T} \quad (3)$$

Using these coordinates in the differential operators the transformed wave equation is

$$\frac{1}{h^2} \nabla^2 \phi - \frac{1}{T^2} \mu \epsilon \ddot{\phi} - \frac{1}{T} \mu \sigma \dot{\phi} = 0 \quad (2B)$$

Multiplying through by h^2 we obtain the final dimensionless form

$$\nabla^2 \phi + C_1 \ddot{\phi} + C_2 \dot{\phi} = 0 \quad (2C)$$

where

$$C_1 = -C^2 \mu \epsilon \quad C_2 = -C \mu \sigma h \quad (4)$$

$$E_x = \frac{\partial \phi}{\partial y}, \quad E_y = -\frac{\partial \phi}{\partial x} \quad (5)$$

and

$$\dot{B}_z = \nabla \times \vec{E} = -\nabla^2 \phi, \quad B(t) = -\int_0^t (\nabla^2 \phi) dt \quad (6)$$

It is assumed that the permittivity, permeability and conductivity of the air above the ground is equal to that of free space. The constants occurring in the propagation equation then become

$$C_{1_{\text{air}}} = -c^2 \mu_0 \epsilon_0, \quad C_{2_{\text{air}}} = 0$$

and

$$C_{1_{\text{ground}}} = -c^2 \mu_0 \epsilon_0 \epsilon_r, \quad C_{2_{\text{ground}}} = c \mu_0 \sigma_2 h \quad (7)$$

The propagation calculation is thus normalized by the relative permittivity of the ground ($\epsilon_r = \epsilon_{\text{ground}} / \epsilon_0$) and $\sigma_2 h$.

The calculated waveforms are plotted against local retarded times in the air and in the ground (τ' and τ'' respectively) in terms of the fundamental time T . These retarded times are based on the optical path from the origin to the point (x, y) and are given (for $x > 0$ and $C_1 > C_2$) by

$$\tau' = \frac{1}{T'} \left(t - \frac{x}{c} \right)$$

$$\tau'' = \frac{1}{T'} \left[t - \frac{x}{c} + \frac{y}{c \sqrt{\epsilon_r - 1}} (1 + \epsilon_r) \right] \quad (8)$$

where t is the real time.

The incident pulse waveform was taken to be a unit step function which was incorporated in the finite difference calculation as a linear ramp with a fast risetime. This incident pulse rises to a unit amplitude and then remains constant. For numerical accuracy it was found that the risetime of this incident rise had to correspond to four or five spatial grids. A risetime much shorter than this would lead to excessive numerical oscillations in the computed values of the field components. The time step in the calculation was taken to correspond to one-third of a spatial grid in order to assure the stability of the calculation.

The numerical oscillations in the computed field components were most prominent below and on the air-ground interface where a finite conductivity exists. These effects are illustrated by figure 2 and 3. Figure 2 shows a typical computed B-field waveform on the air-ground interface where the numerical oscillations are most pronounced. This figure shows the diminution in the amplitude and period of the numerical oscillations when the spatial and time grid sizes were reduced for a given risetime.

Computational experiments with the use of a finer mesh in the calculation indicated that the results tended to converge to a value midway between the extremes of the oscillations encountered with a coarser mesh.

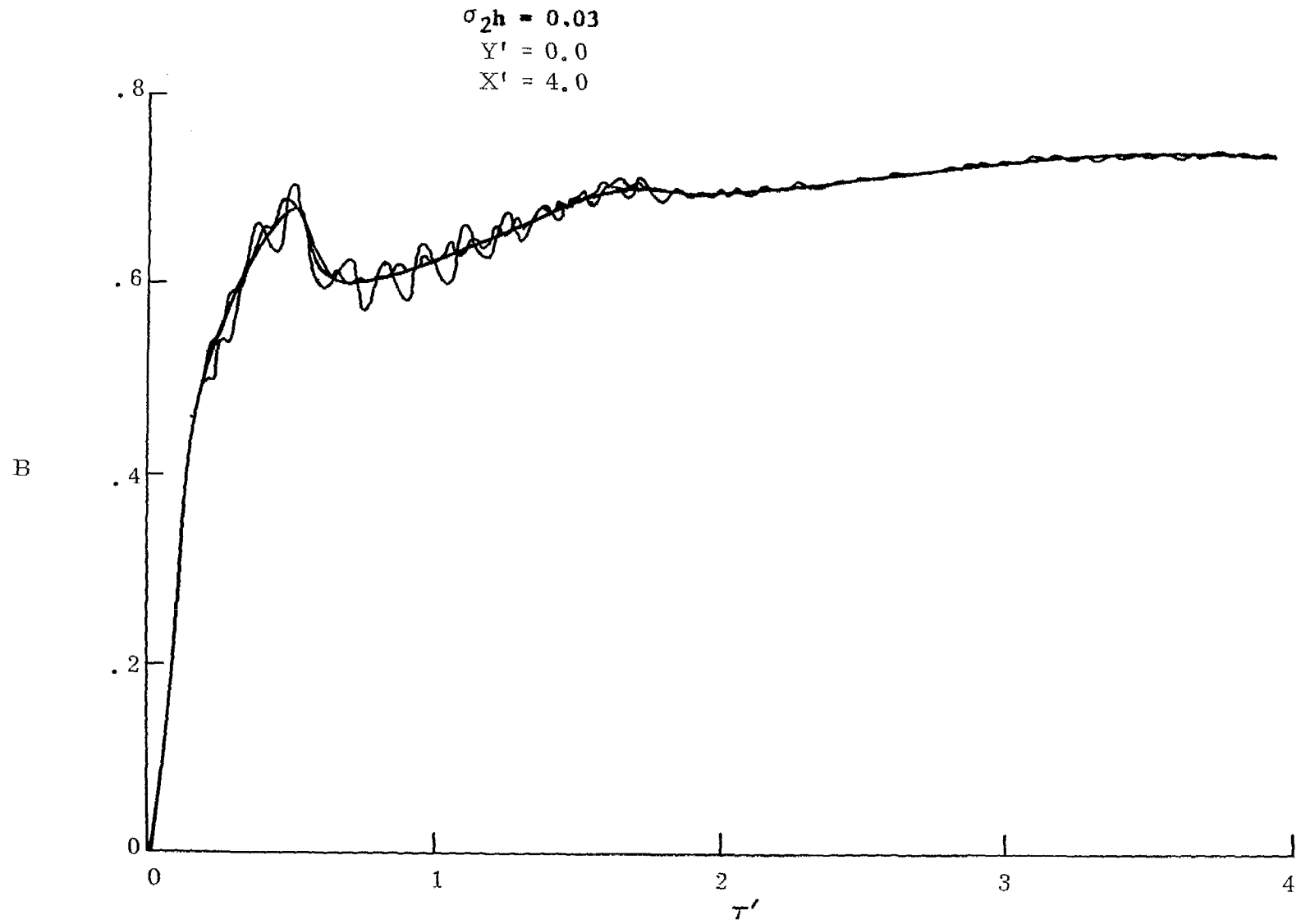


Figure 2. Illustration of Numerical Oscillations at the Interface with Various Space Time Grids and Their Converging to the Smoothed Results.

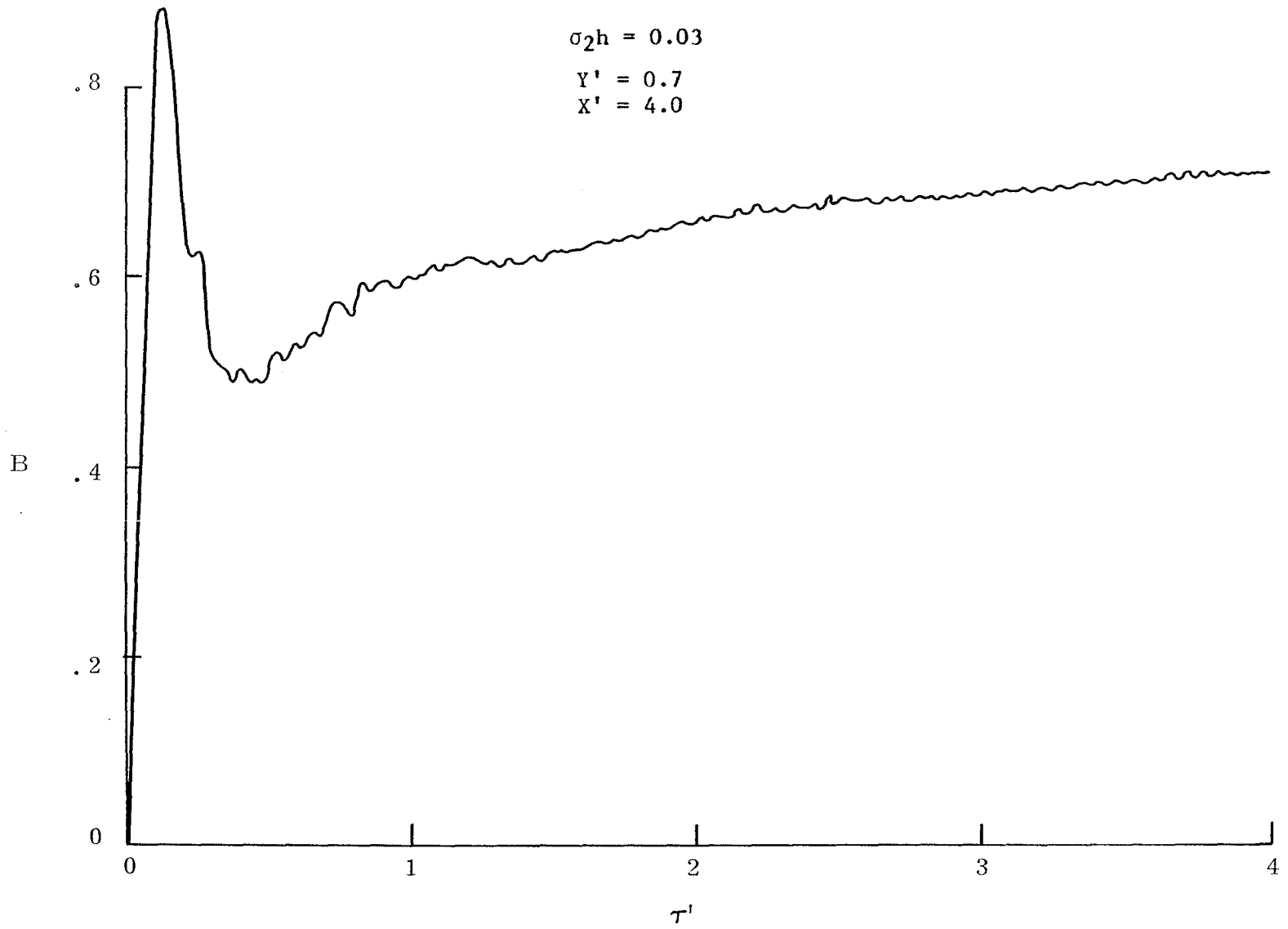
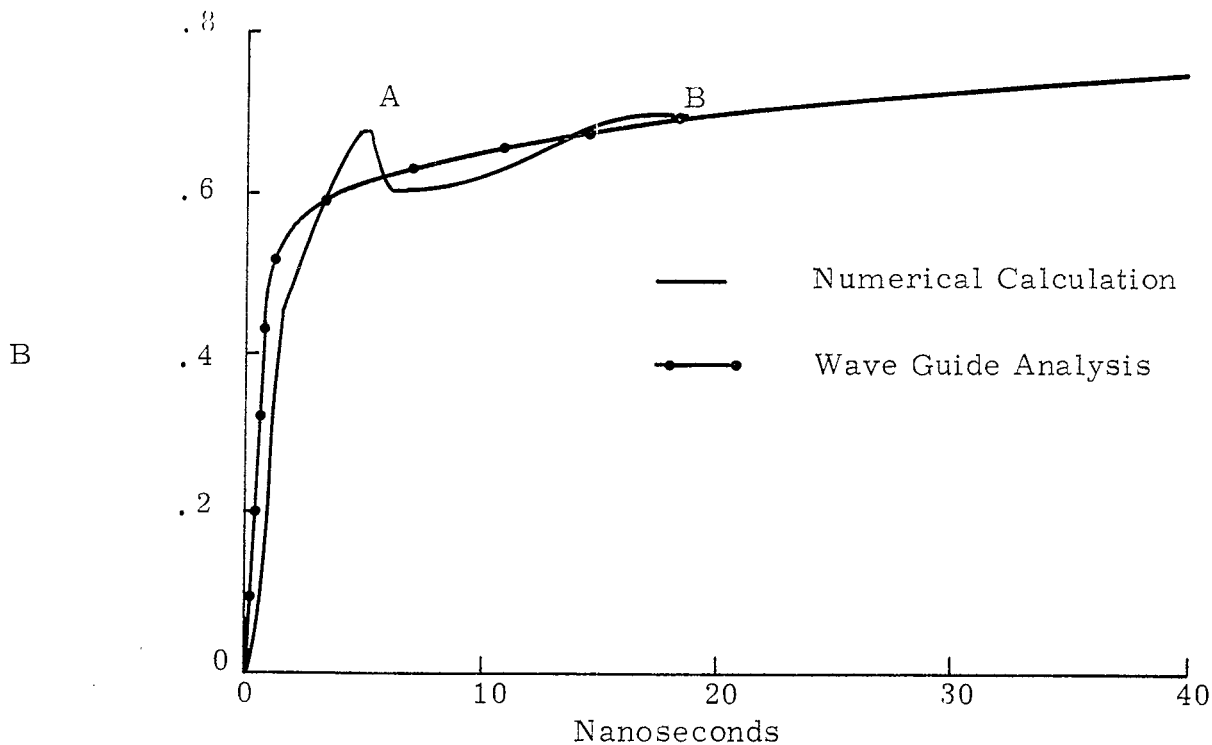


Figure 3. Magnitude of Oscillations Above Interface.

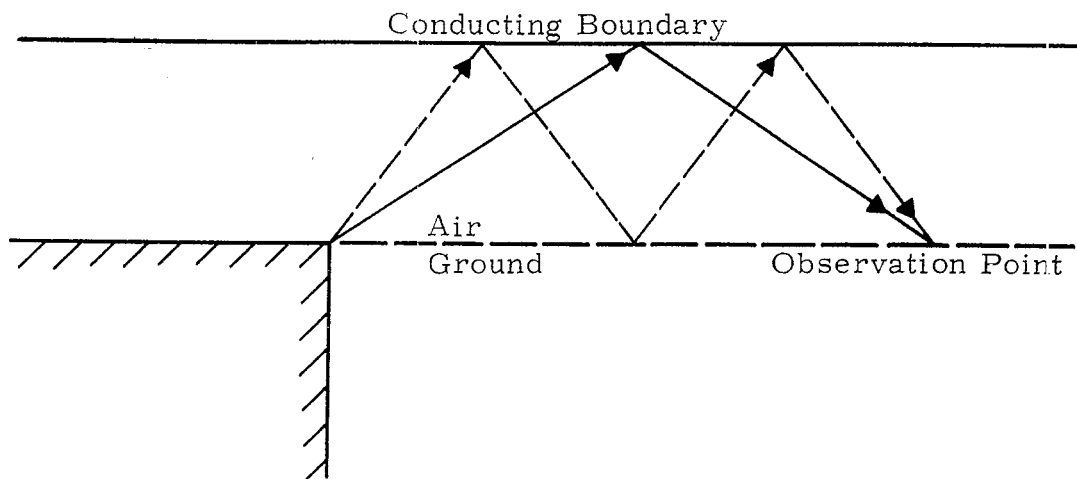
This effect is illustrated in figure 2. In view of this convergence, the numerical results were fitted with a smooth curve through the center of the oscillations. To minimize the inaccuracies in this procedure without using excessive computer time the calculations were carried out to time $\tau' = 1.0$ using a spatial grid size $\Delta x' = \Delta y' = \Delta s = .01$. This time range encompasses the risetime, that part which is most rapidly changing, of the waveform. The calculations were completed to later times ($\tau' > 1.0$) using $\Delta s = .01667$.

Figure 3 shows a typical B-field waveform computed above the air-ground interface and illustrates less pronounced numerical oscillations relative to calculations on and below this interface. Therefore, the inaccuracies involved in fitting a smooth curve through these points is less than that involved in smoothing the computed waveforms on and below the interface. As can be judged from these typical examples, the smoothed results presented in this note represent the converged values of the waveform to within a few percent, the greatest error occurring where the rate of change is greatest.

The inflection in the waveforms at point A in figure 4-A arises from the diffracted wave formed at the ground/conductor interface and then reflecting off the top plane to the observation point. The second inflection at B corresponds to the first multiple reflection from the top conductor and then the ground surface arriving at the observation point. These reflection paths are illustrated in figure 4-B. These reflection effects are most prominent in the results given for E_y since this component arises directly from the diffraction that alters the incident plane wave pulse.



A. Waveform Inflections Resulting from Reflection.



B. Reflection Paths to Observation Point.

Figure 4. Early Time Reflection Characteristics.

III. Waveguide Model

The waveguide model used for calculations presented in this note is an extension of the method given by Baum^{2, 3} to allow calculations of some response characteristics above and below the air ground interface. The waveguide solutions are computed in the frequency domain for an incident pulse having a fast risetime comparable with that used in the finite difference calculation. These results are then used to generate the time domain waveforms by means of a numerical calculation of the inverse fourier transform.

This method allows the relatively rapid computation of the field waveforms in an approximation that comes into more exact agreement with the finite difference results at lower frequencies (later times).

The coordinate system of the geometry of the transmission line is illustrated in figure 1-B. Note that the coordinate system in Section II differs somewhat from the system in this section. That is, the y and z directions in figure 1-B correspond to the z and y directions respectively in figure 1-A. The length of the transmission was set to a value of $x = d$ such that no reflections from the termination would occur within the time frame of interest in the comparisons presented here. The electrical parameters permittivity, permeability and conductivity (ϵ , μ and σ respectively) above the air-ground interface are assumed to be the same as those of free space. Below the interface the ground is assumed to have permittivity ϵ_2 , permeability μ_0 and conductivity σ_2 . The relative permittivity is defined as $\epsilon_r = \epsilon_2 / \epsilon_0$.

The equations for the fields above the air-ground interface
($0 < z < h$) from reference 2 are

$$\tilde{E}_{z_1} = -\frac{\gamma_x}{\gamma_1} Z_1 \tilde{B} \cosh(\gamma_{z_1} z') e^{-\gamma_x x} \quad (9)$$

$$\tilde{E}_{x_1} = -\frac{\gamma_{z_1}}{\gamma_1} Z_1 \tilde{B} \sinh(\gamma_{z_1} z') e^{-\gamma_x x} \quad (10)$$

$$\tilde{H}_{y_1} = \tilde{B} \cosh(\gamma_{z_1} z') e^{-\gamma_x x} \quad (11)$$

and the fields below the air-ground interface are

$$\tilde{E}_{z_2} = -\frac{\gamma_x}{\gamma_2} Z_2 \tilde{B} \cosh(\gamma_{z_1} h) e^{\gamma_{z_2} z - \gamma_x x} \quad (12)$$

$$\tilde{E}_{x_2} = \frac{\gamma_{z_1}}{\gamma_1} Z_1 \tilde{B} \sinh(\gamma_{z_1} h) e^{\gamma_{z_2} z - \gamma_x x} \quad (13)$$

$$\tilde{H}_{y_2} = \tilde{B} \cosh(\gamma_{z_1} h) e^{\gamma_{z_2} z - \gamma_x x} \quad (14)$$

Equations for the coefficients γ_x , γ_1 , γ_2 , γ_{z_1} and γ_{z_2} are not repeated here but appear in the references.

The solution of equations 9 and 11 is thoroughly discussed and solved for a wide range of parameters in reference 3. All of the previous studies were for the case along the air-ground interface ($z = 0^+$). However, the other field components above and below the interface can be solved. This can be accomplished, using the solution and computer code for that solution for equations 9 and 11, by taking the ratio of an unknown component to that of a known one. The time domain waveform is then

produced as in the references by an inverse Fourier transform. It should be noted that the field components e_z and h_y do not vary in the range $0 < z < h$ and appear as such in the graphs. The e_x field component varies only with $z' = z - h$ where z is the height above the interface where the calculation is taken and h is the height of the simulator (upper metallic boundary) above the interface.

For the purpose of the comparison a non zero risetime was added to the incident wave. This finite risetime is assumed to be of the form

$$\left[1 - e^{-\zeta \frac{t}{t_d}} \right] u(t) \quad (15)$$

where $\zeta = \frac{t_d}{\text{time constant of the rise}}$ (16)

For the comparisons in this note the time constant was chosen to give a one nanosecond risetime in the incident wave. A retarded time factor as given in equation 8 was incorporated for the calculation of points below the air-ground interface.

IV. Results and Comparisons

A wide range of parameters are used in this comparative parameter study. Specifically these are

$$\sigma = 10^{-1}, 10^{-2}, 10^{-3}, 10^{-4} \text{ mho/meter} \quad (17)$$

$$h = 3 \text{ meters}$$

$$Y' = .7, .5, .2, +0, -0, -.3$$

$$X' = 1, 2, 4, 6, 9, 12, 15 \text{ (except as noted below)}$$

$$\epsilon_r = 10$$

Note that σ (as given on the graphs) is equal to σ_2 for h equal to 3 meters, however, other combinations of σ_2 and h can be chosen to satisfy equation 7. The graphs in Appendix A are subdivided first by conductivity, the heading of each page, and secondly by Y' , the heading of each graph. On each graph X' is defined by the number to the right of the termination of the curve. In some cases the value of X' appears above the peak of the curve if the curves converge as τ' increases. Waveforms from both methods of calculation appear on the graph with curves marked with "O" indicating waveforms computed by the waveguide model. Three comparisons are made on each graph, namely $Y' = 1, 6$ and 15 . The other waveforms were not compared to avoid undue confusion.

In general for times $\tau' > 1$ and $\tau'' > 1$ agreement between the waveforms of the two methods is good. In making the comparison it should be noted that there are some general restrictions on the ranges of the various parameters for the waveguide model. These restrictions are

$$\left[10.4 \epsilon_r Z_0^2 h^2 \sigma_2^2 \right]^{-1} \ll 1 \quad (18)$$

and

$$\omega \ll \frac{c\sqrt{\epsilon_r}}{h} \quad (19)$$

where Z_0 is the wave impedance of free space.

A summary of the parameters used for the graphs in this note are tabulated in Table 1. Since the graphs are not numbered sequentially but are grouped according to their major parameters. Each graph has seven values of X' (1, 2, 4, 6, 9, 12 and 15) except those marked with an asterisk which have only 1, 6 and 15 due to the density of the curves.

σ	Y'	B	E_y	E_x
10^{-1}	.7	A2	A4	A5*
	.5	A2	A4	A5*
	.2	A2	A4	A5*
	+0	A2	A4	A5*
10^{-2}	-0	A3	A4	A5*
	-.3	A3	A4	A5*
	.7	A6	A8	A9
	.5	A6	A8	A9
10^{-3}	.2	A6	A8	A9
	+0	A6	A8	A9
	-0	A7	A8	A9
	-.3	A7	A8	A9
10^{-4}	.7	A10	A12	A13
	.5	A10	A12	A13
	.2	A10	A12	A13
	+0	A10	A12	A13
10^{-3}	-0	A11	A12	A13
	-.3	A11	A12	A13
	.7	A14	A16	A17
	.5	A14	A16	A17
10^{-4}	.2	A14	A16	A17
	+0	A14	A16	A17
	-0	A15	A16	A17
	-.3	A15	A16	A17

Table 1. Summary of Location of Graphs by Major Parameters
(all units rationalized MKSA)

V. References

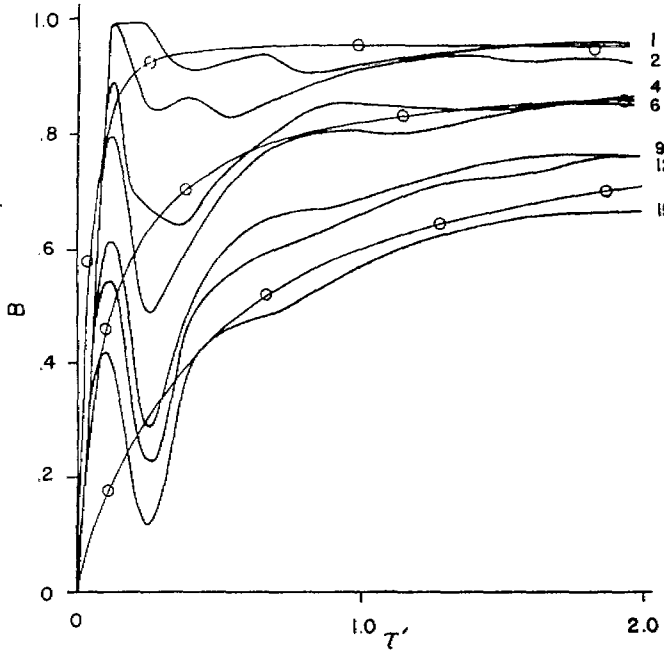
1. W. E. Page and D. H. Peterson, Sensor and Simulation Note 96, A Numerical Method for Computing the Propagation of an Electromagnetic Pulse Guided Over a Material Interface, January 1970.
2. C. E. Baum, Sensor and Simulation Note 46, The Single-Conductor, Planar, Uniform Surface Transmission Line, Driven from One End, July 1967.
3. C. E. Baum, Sensor and Simulation Note 92, A Parameter Study of the Uniform Surface Transmission Line Driven by a Step Function Voltage and Terminated in its High-Frequency Characteristic Impedance, August 1969.

Appendix A

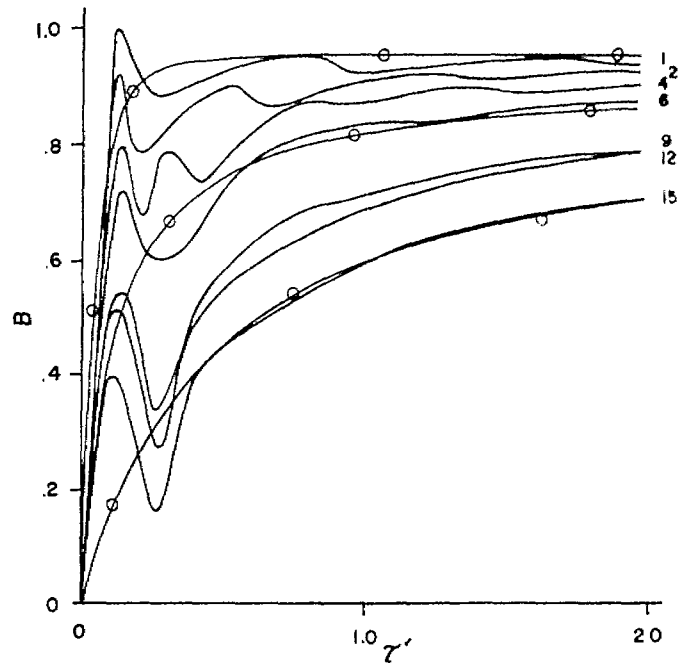
Graphs for the Comparitive Parameter Study

$\sigma = 0.1$

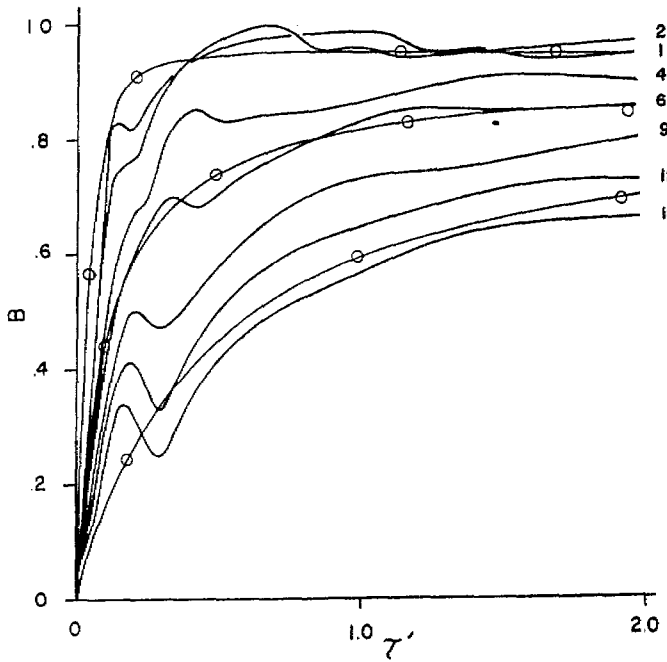
$\gamma' = 0.7$



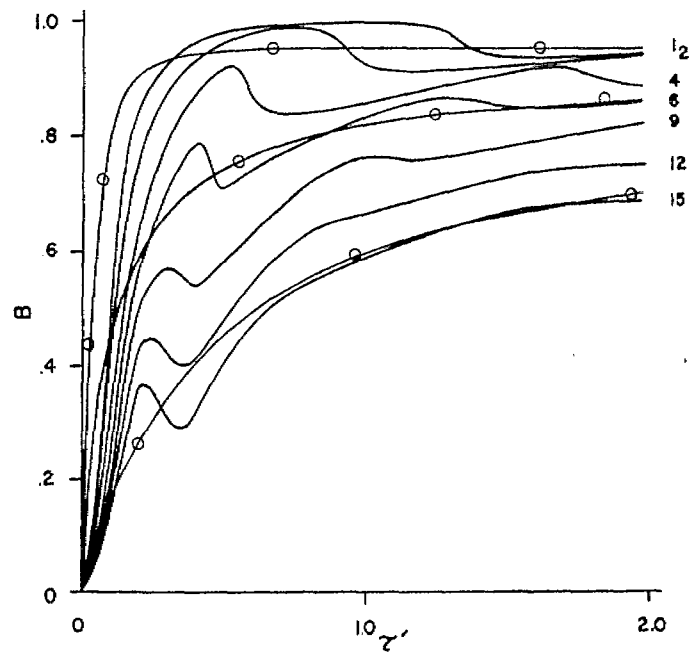
$\gamma' = 0.5$



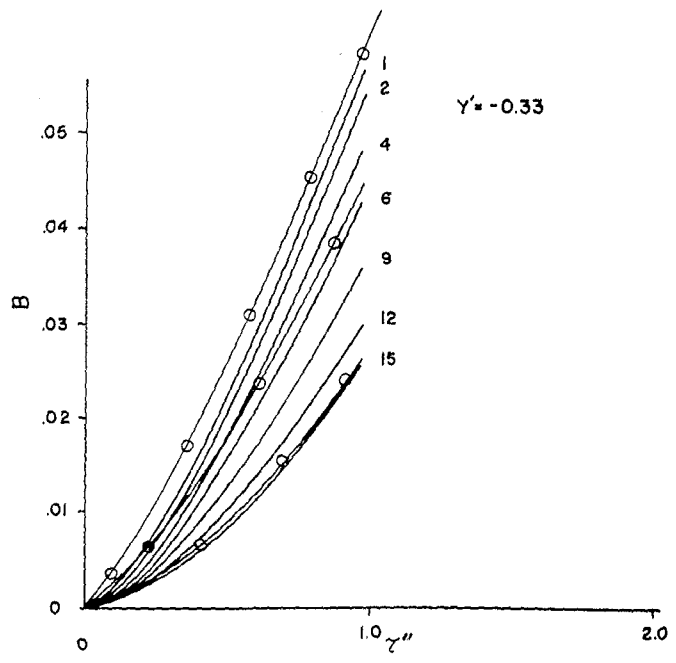
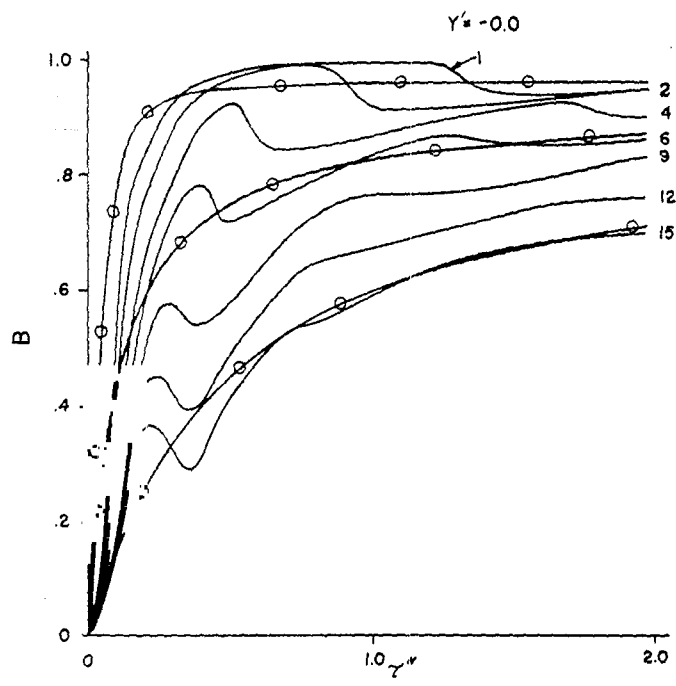
$\gamma' = 0.2$



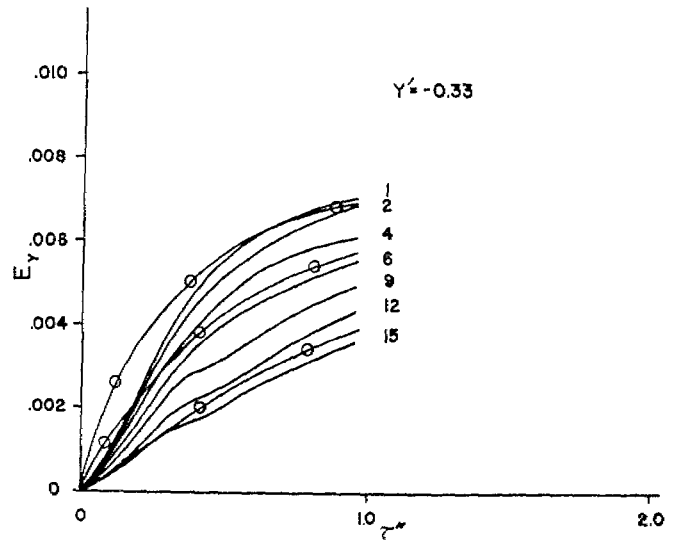
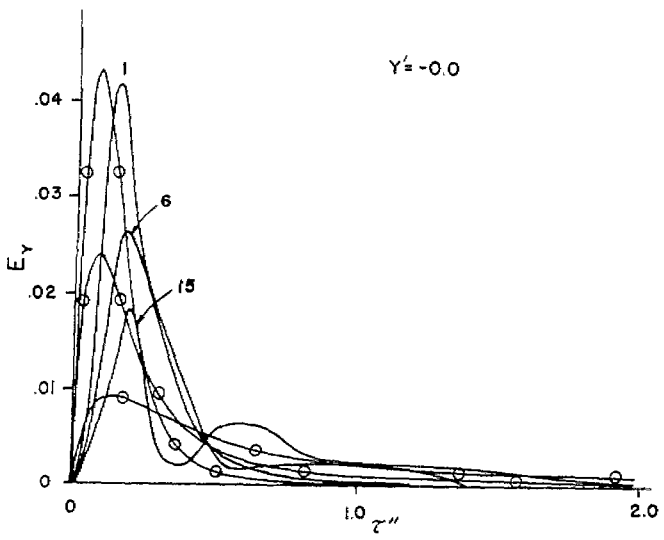
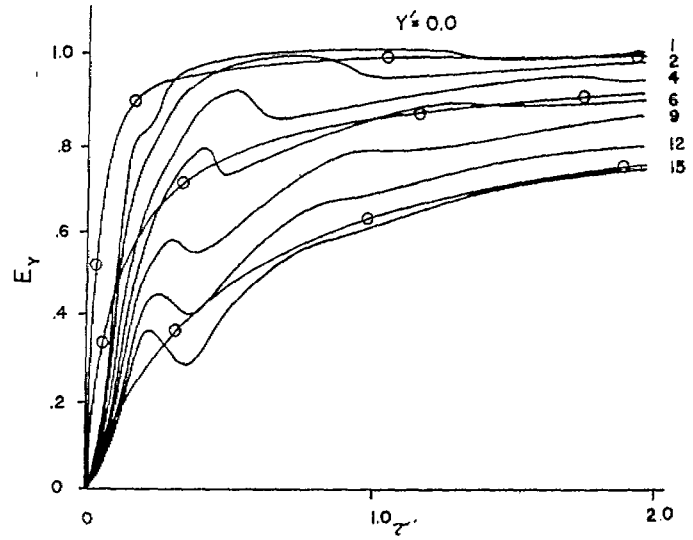
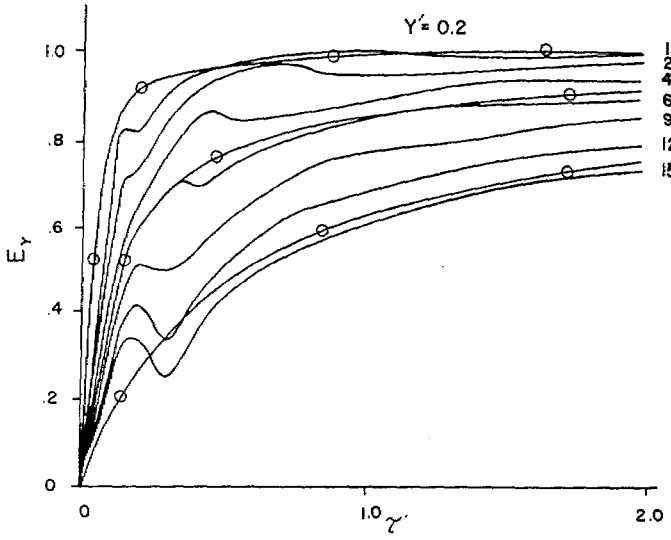
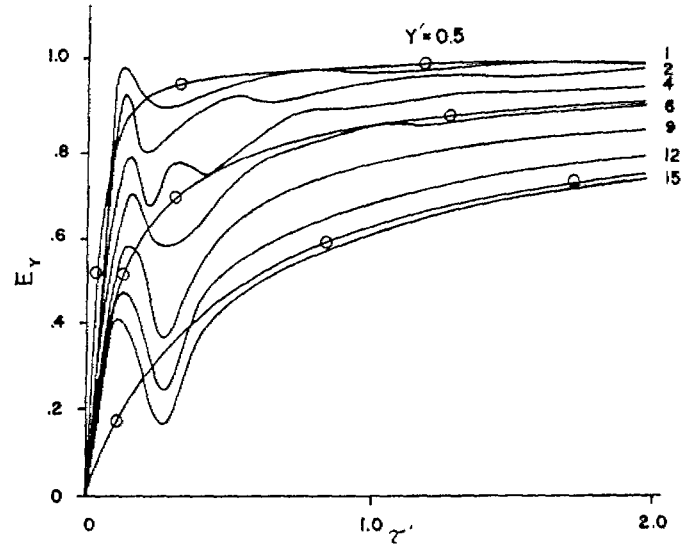
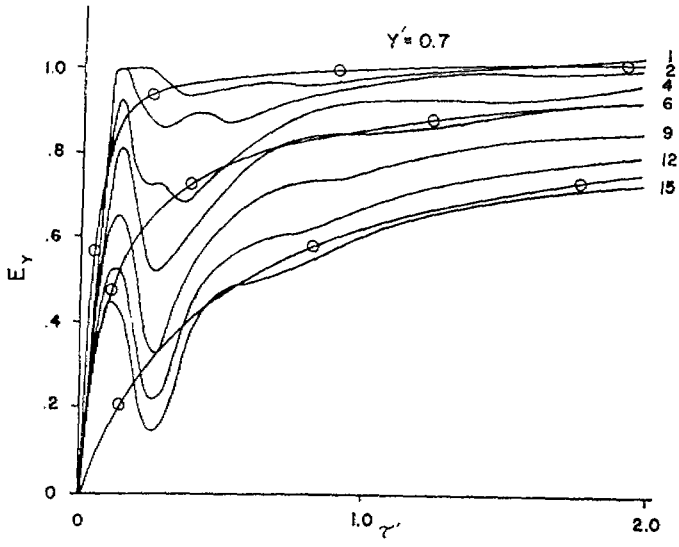
$\gamma' = 0.0$



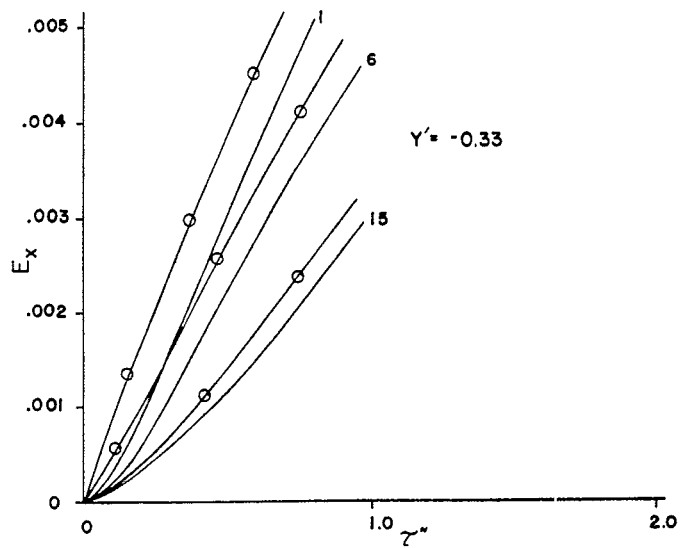
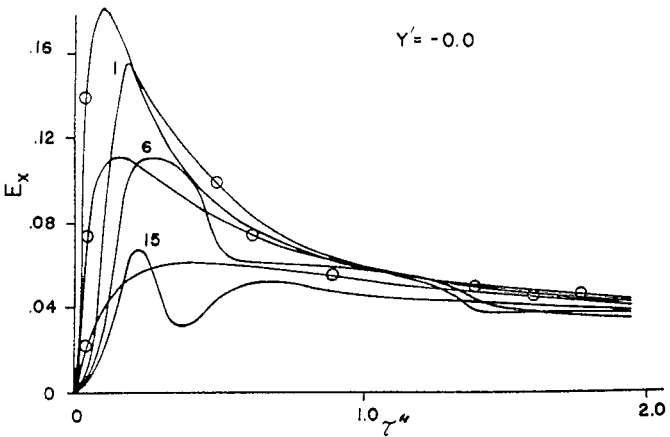
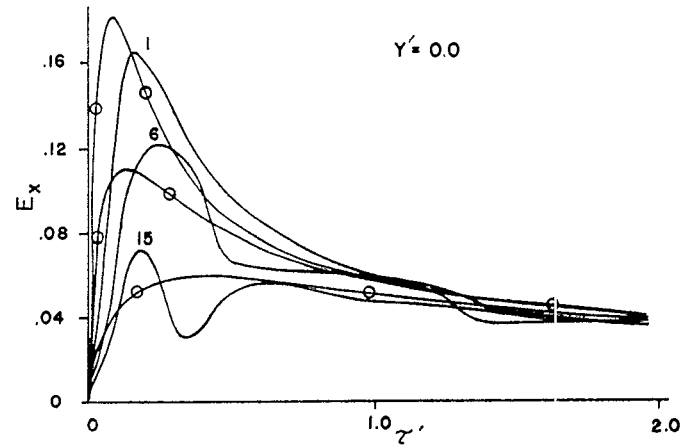
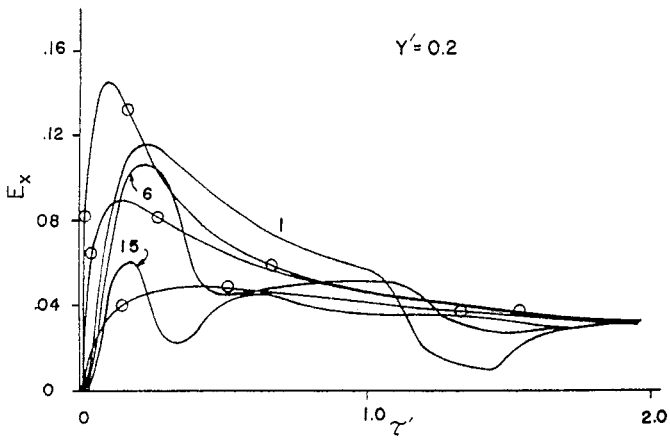
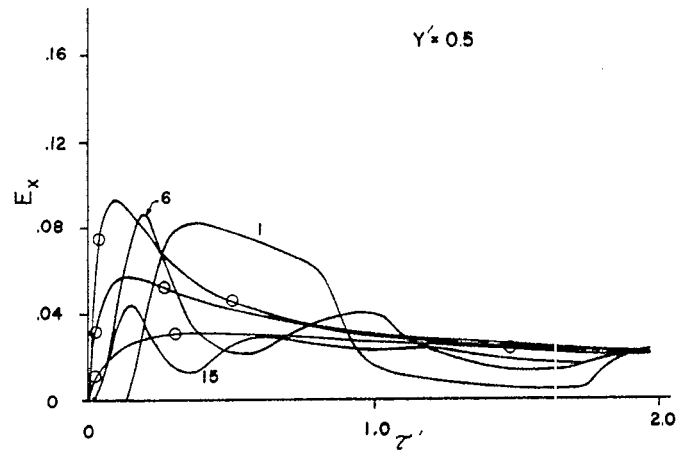
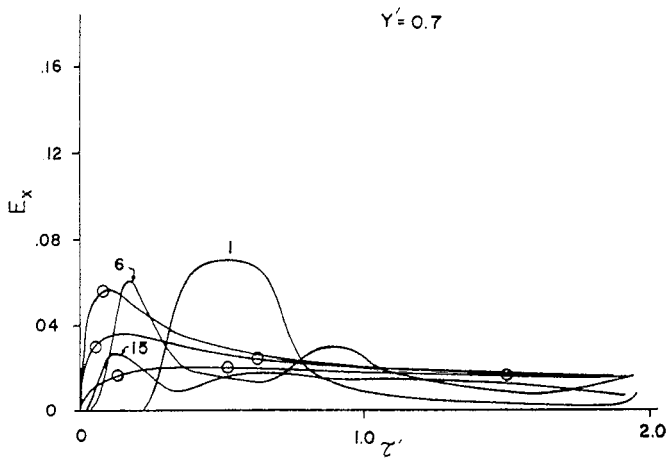
$\sigma = 0.1$



$\sigma = 0.1$

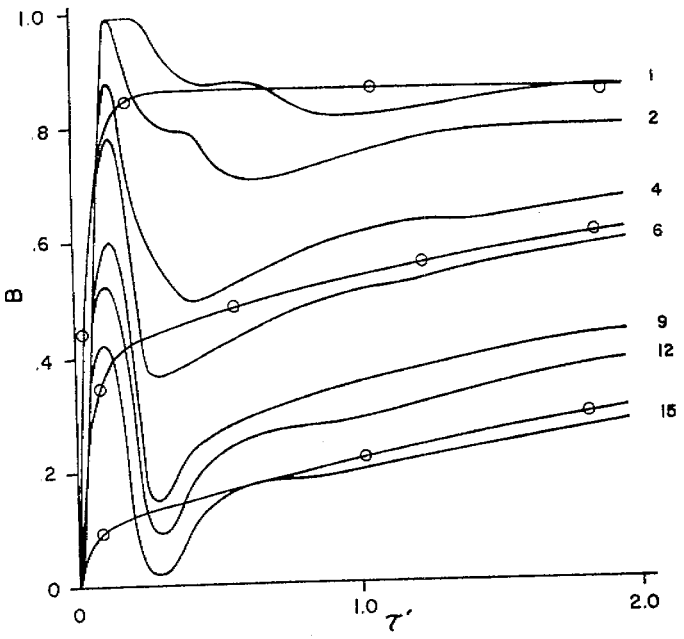


$\sigma = 0.1$

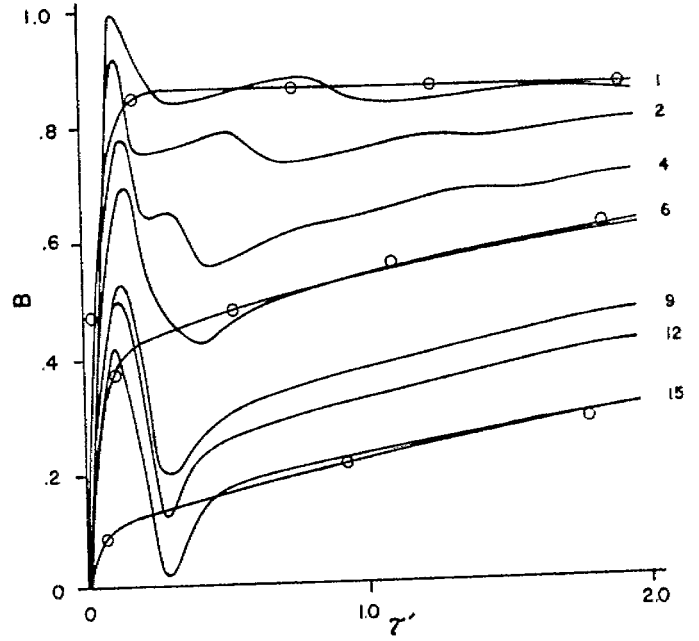


$\sigma = 0.01$

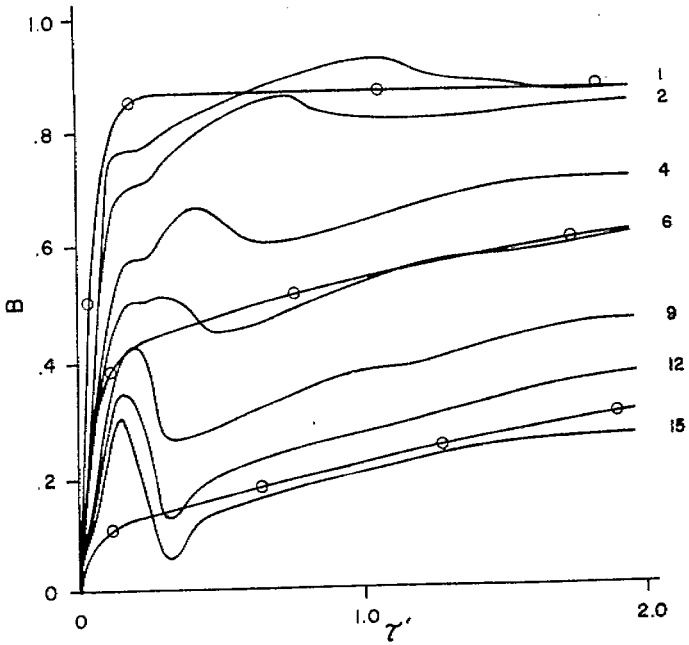
$\gamma' = 0.7$



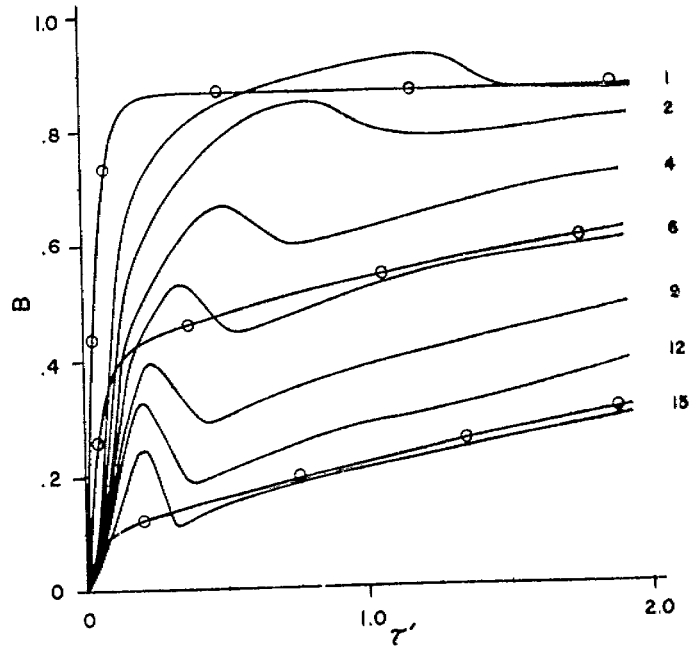
$\gamma' = 0.5$



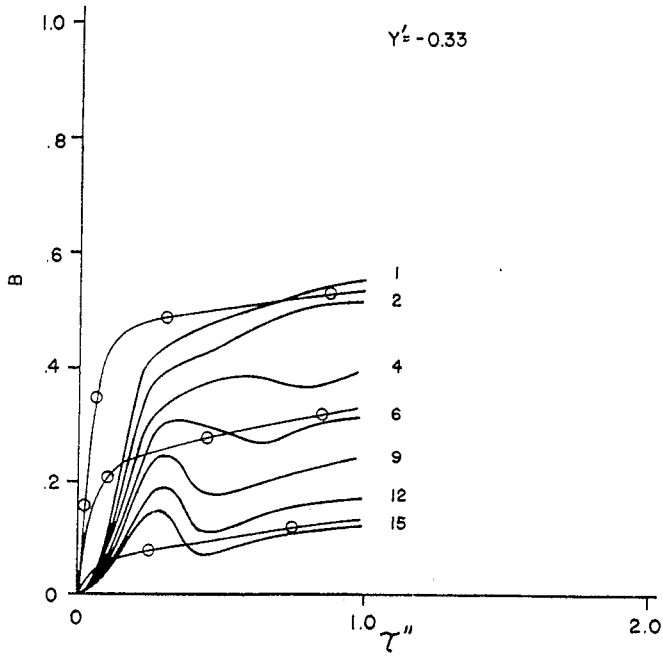
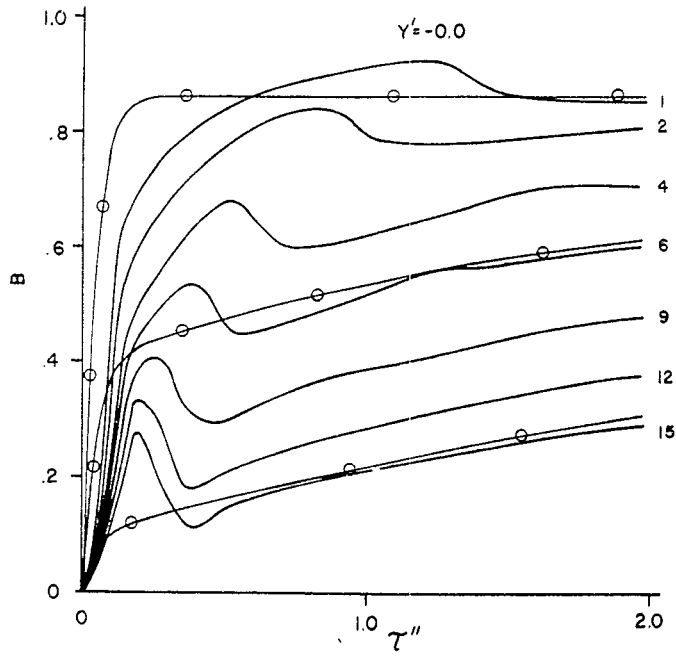
$\gamma' = 0.2$



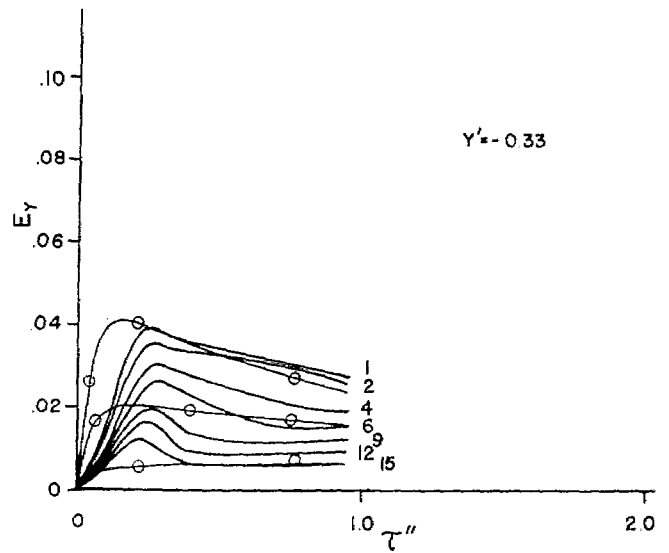
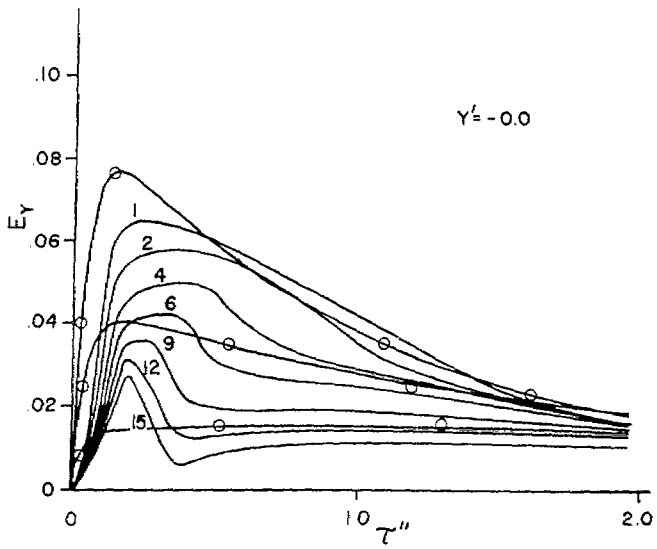
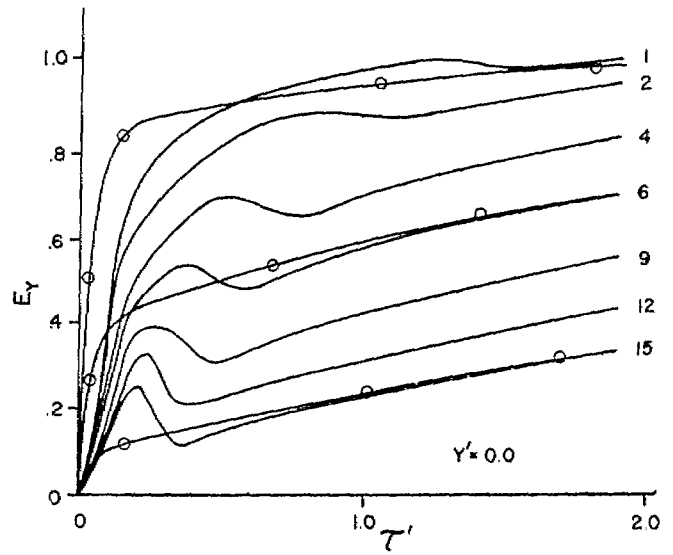
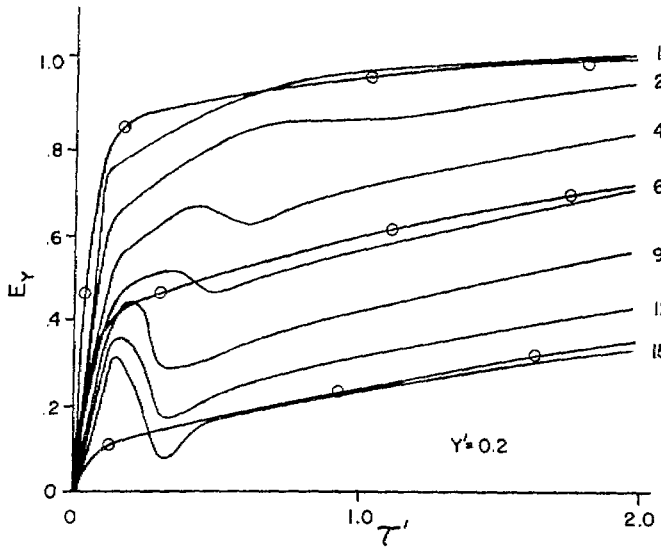
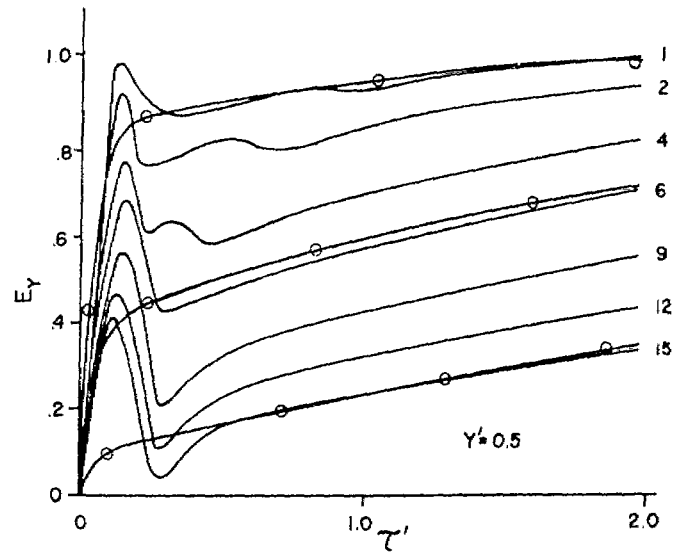
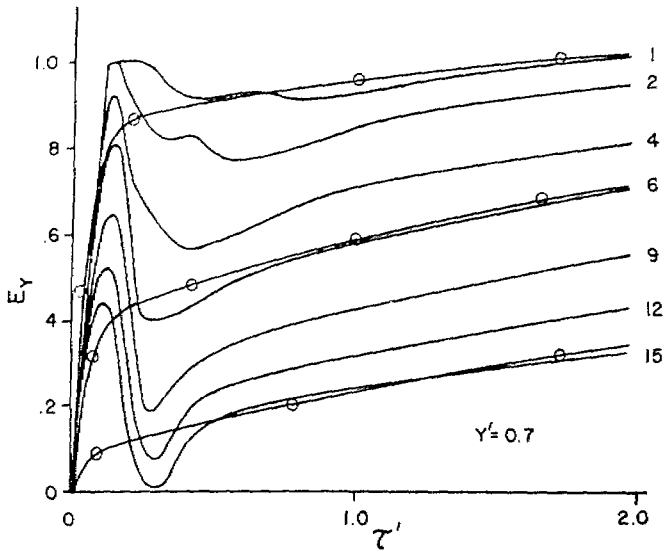
$\gamma' = 0.0$



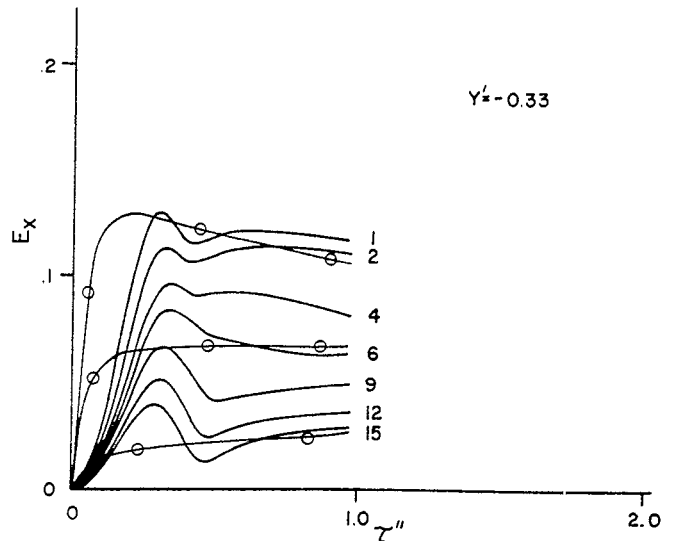
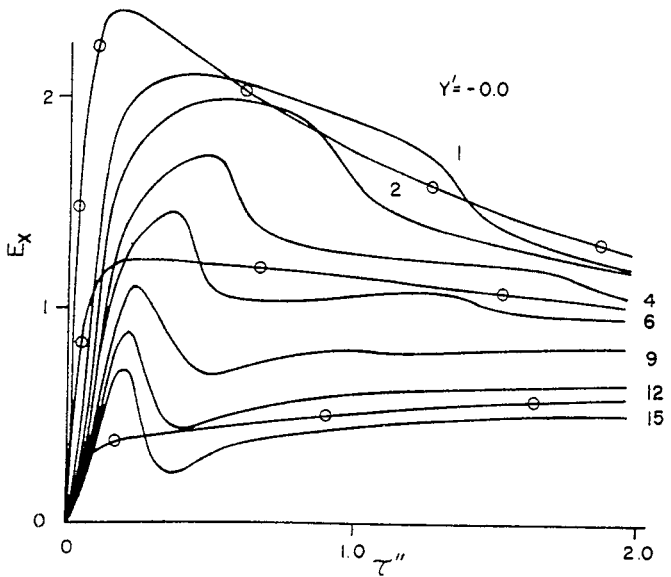
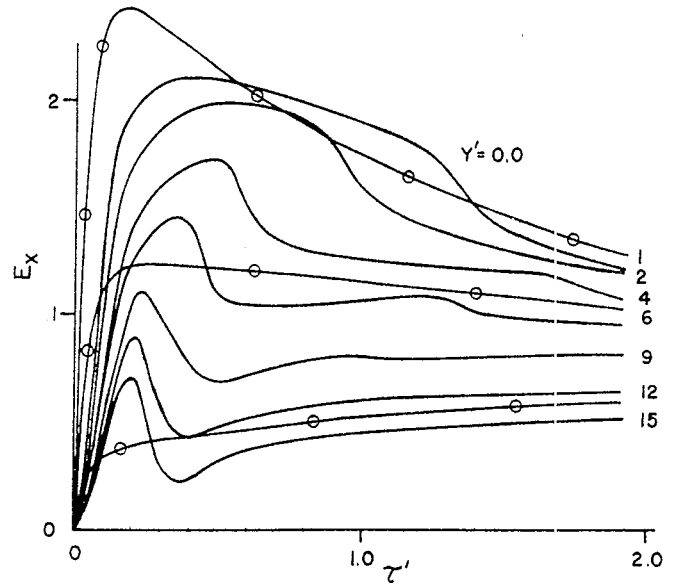
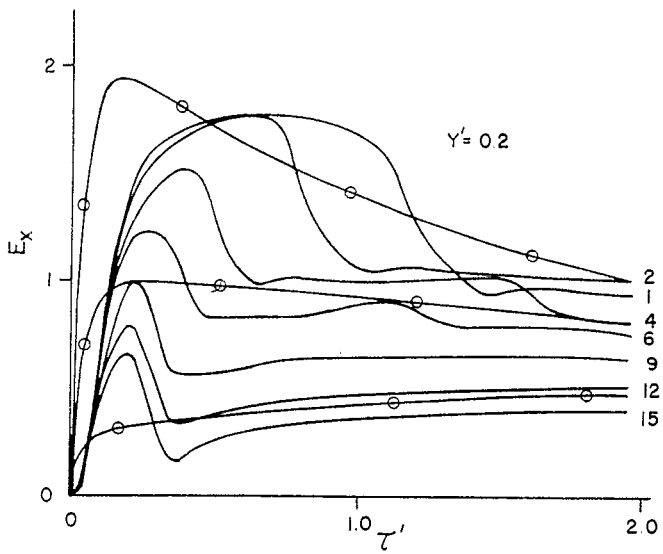
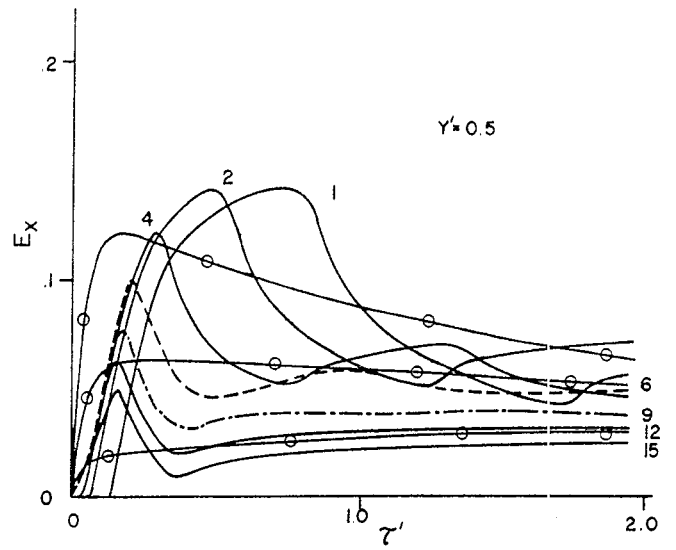
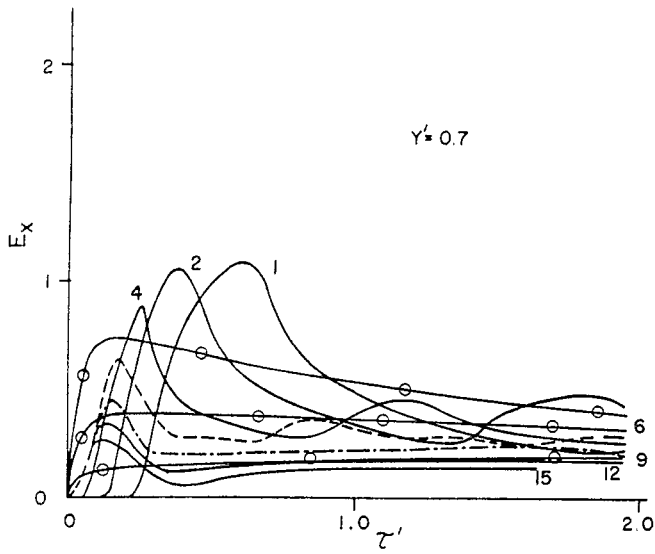
$\sigma = 0.01$



$\sigma = 0.01$

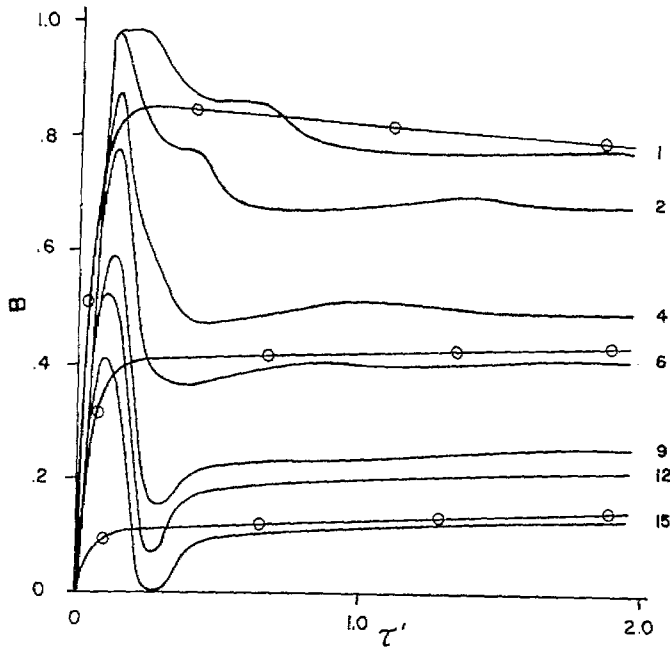


$\sigma = 0.01$

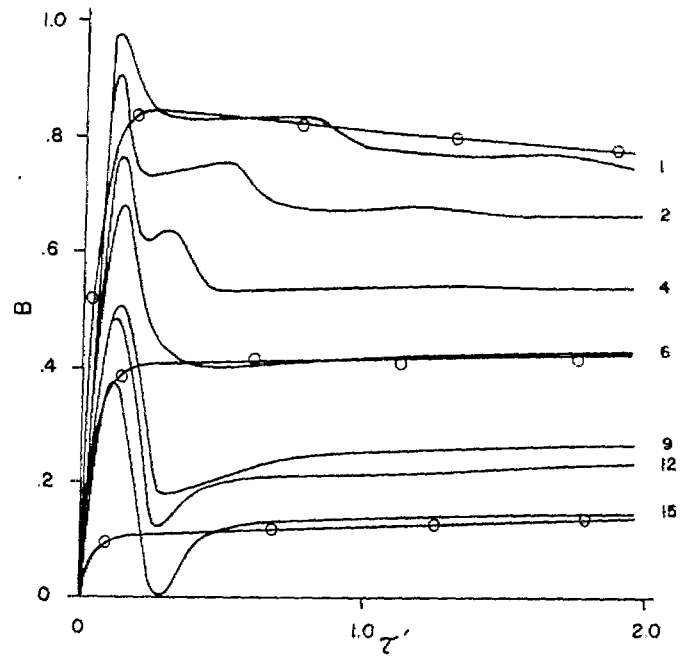


$\sigma = 0.001$

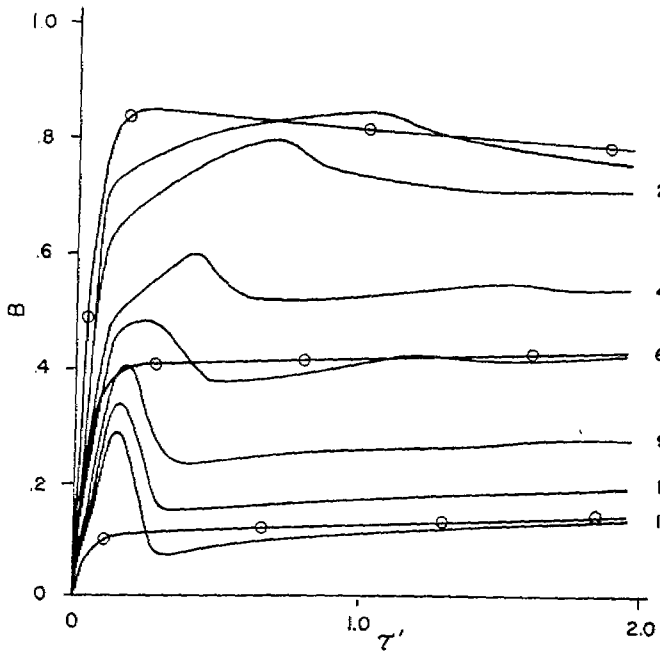
$\gamma' = 0.7$



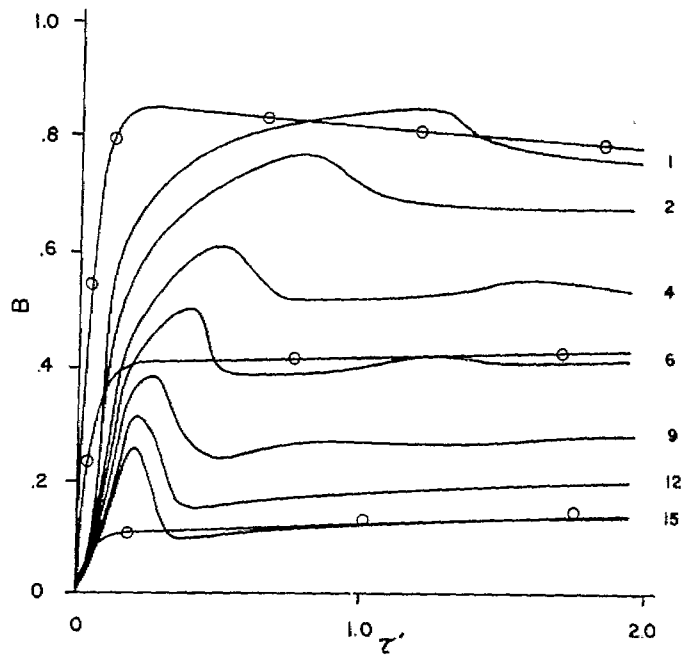
$\gamma' = 0.5$



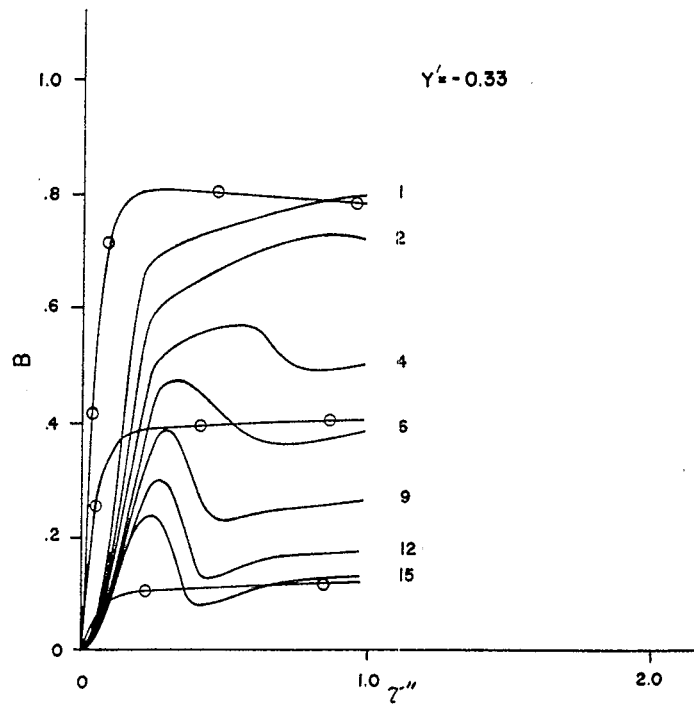
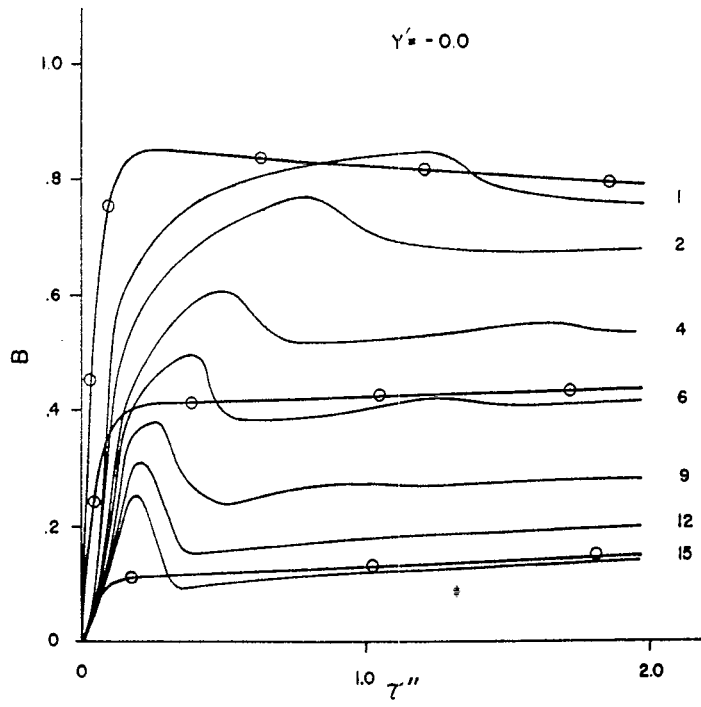
$\gamma' = 0.2$



$\gamma' = 0.0$

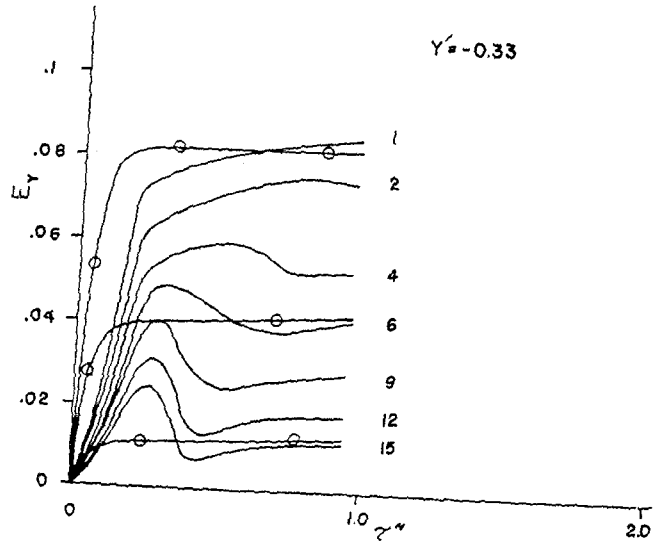
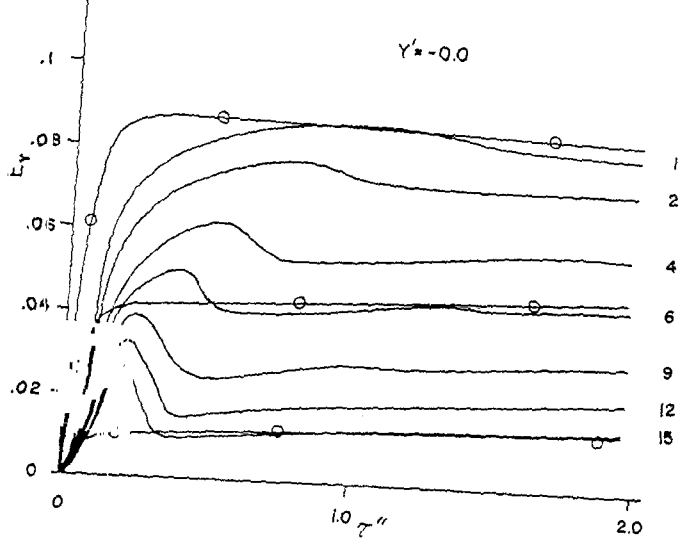
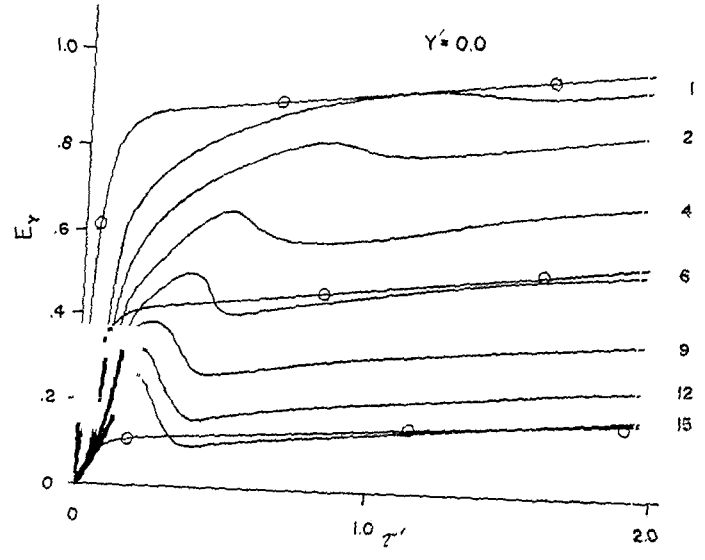
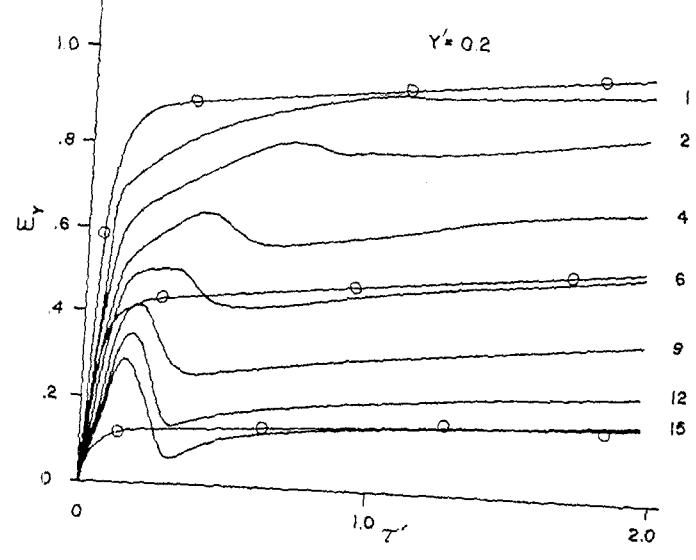
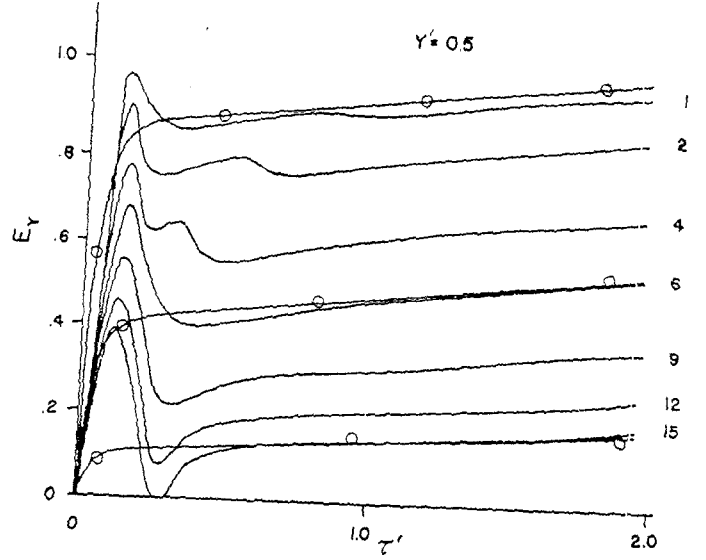
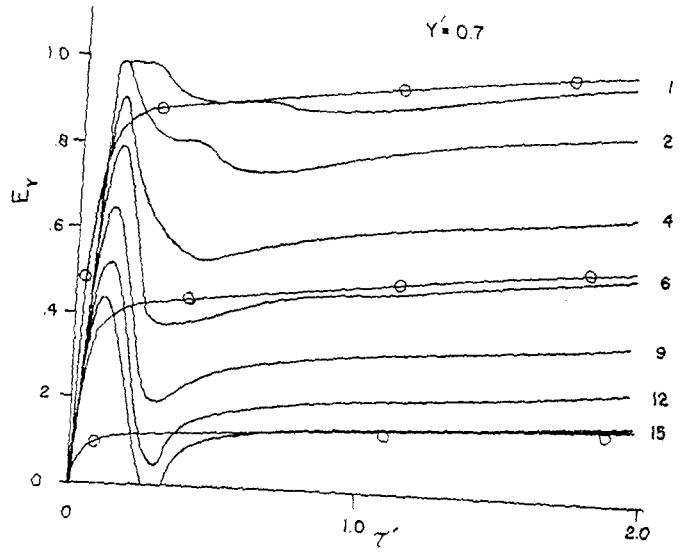


$\sigma = 0.001$

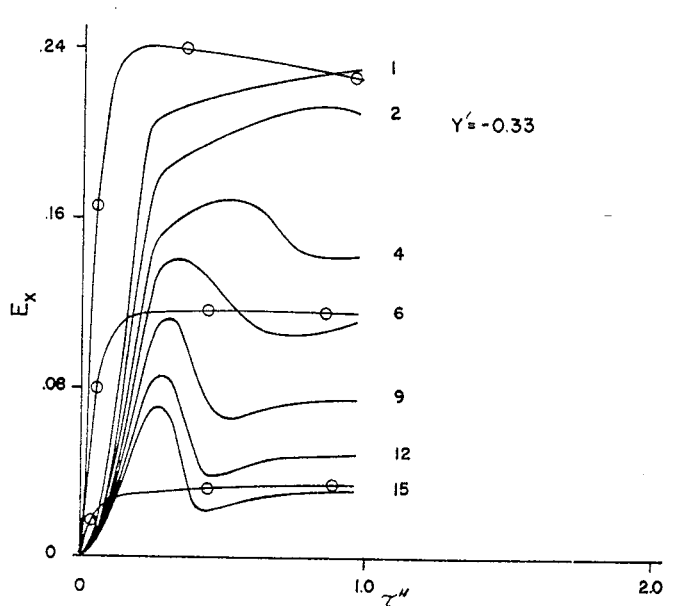
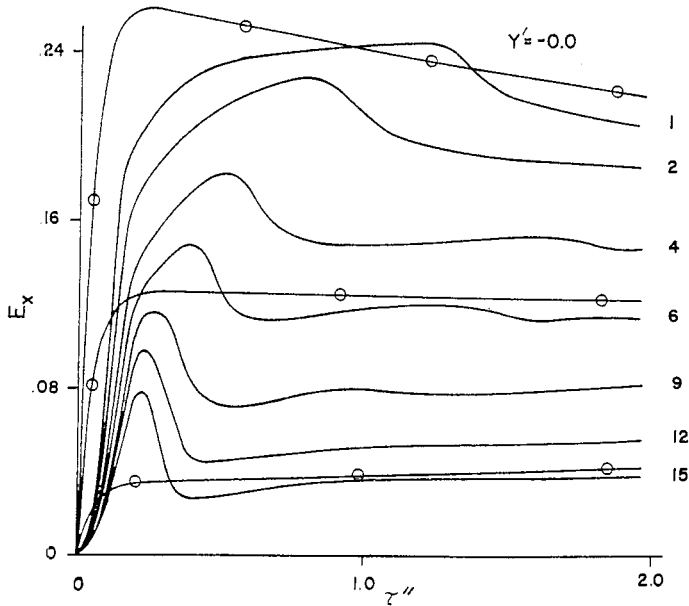
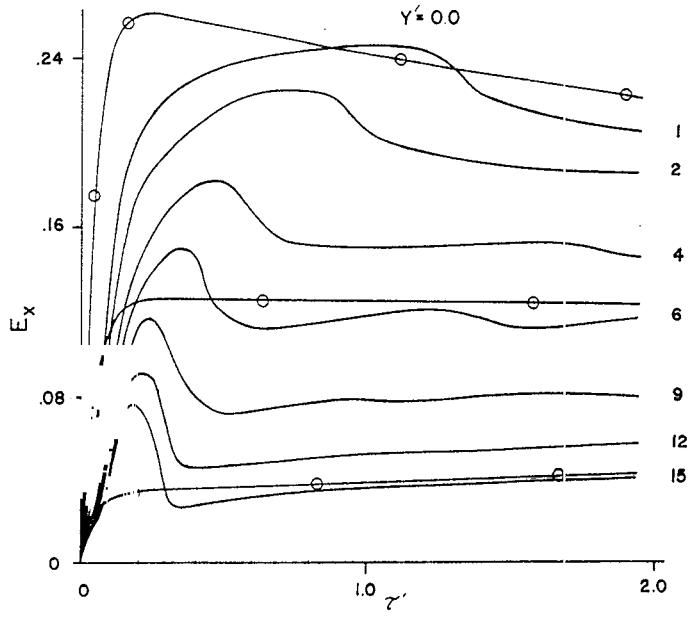
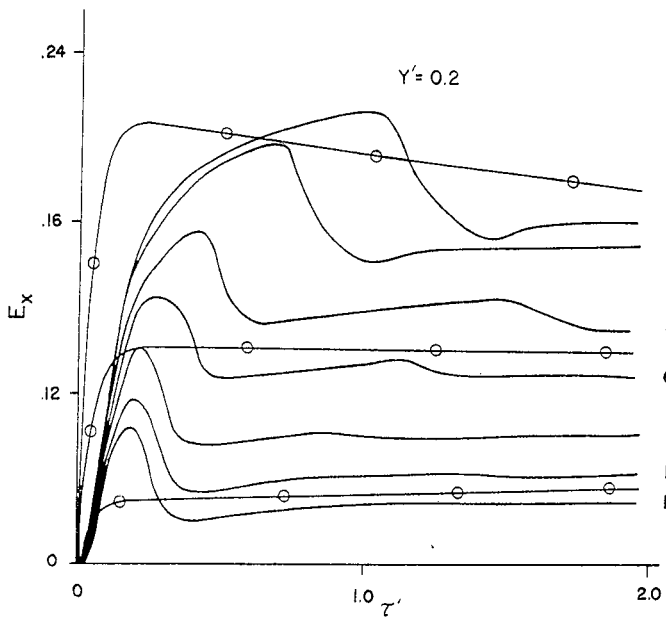
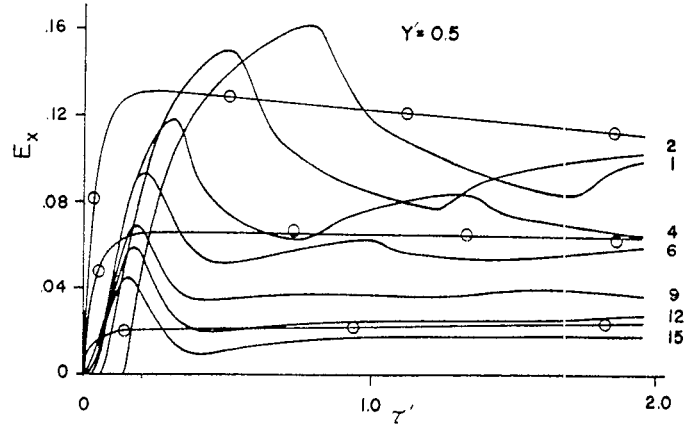
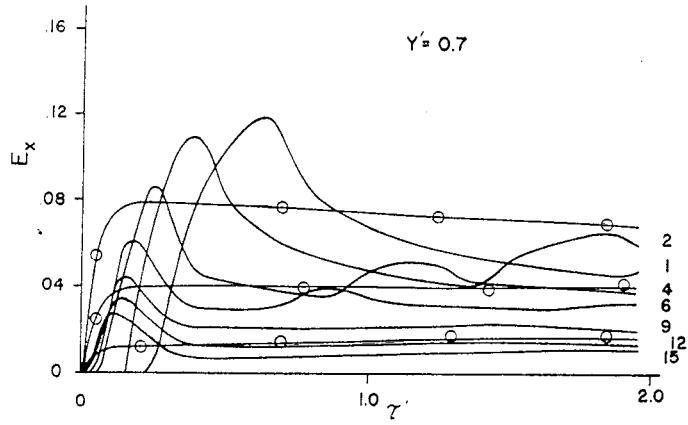


A11

$\sigma = 0.001$

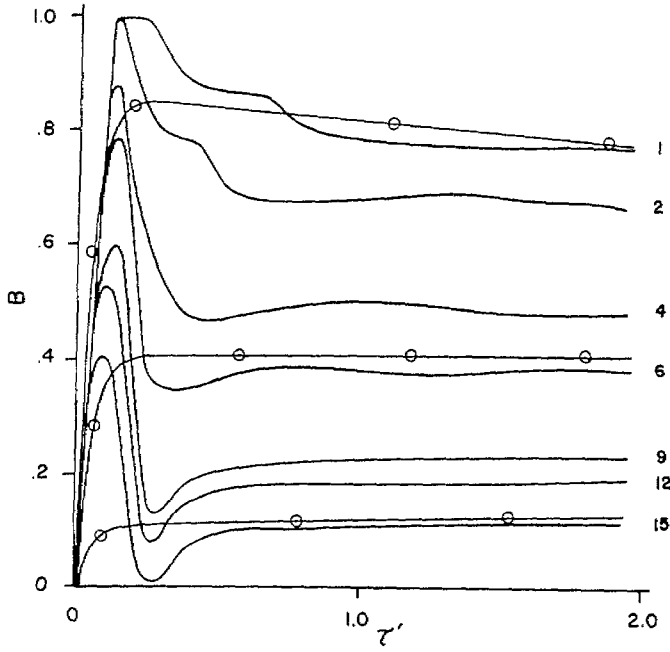


$\sigma = 0.001$

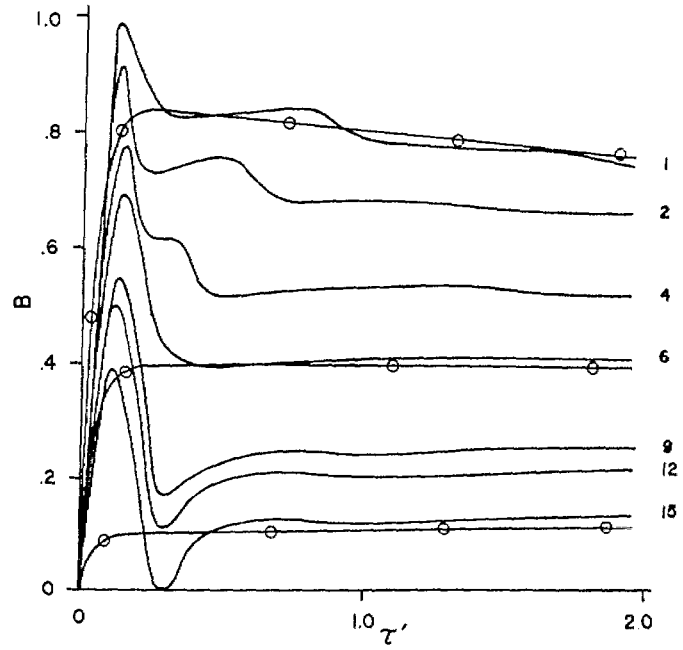


$\sigma = 0.0001$

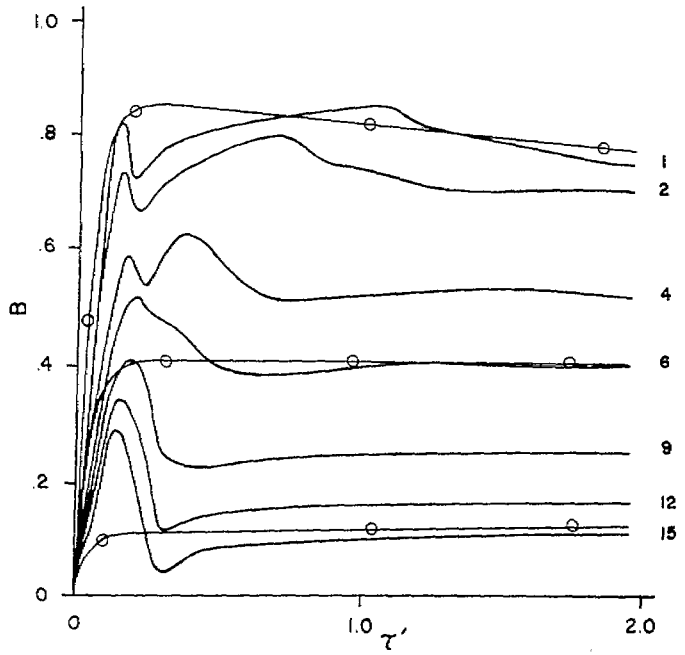
$\gamma' = 0.7$



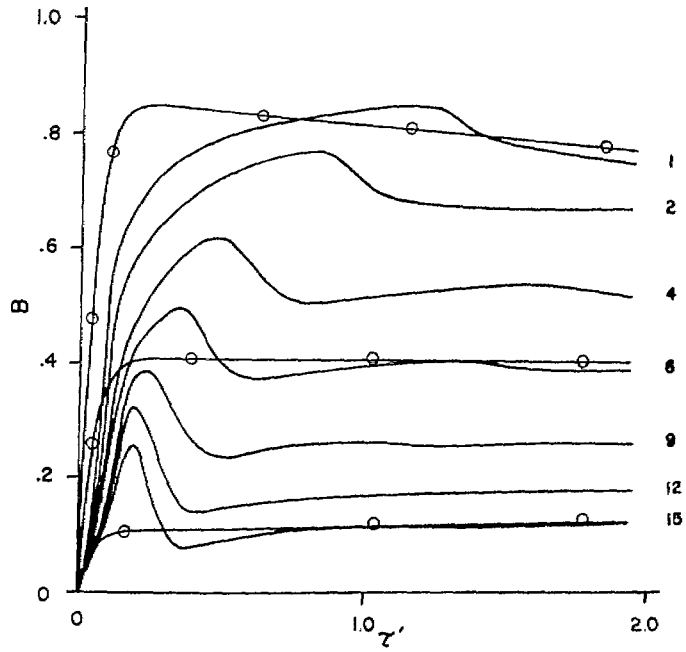
$\gamma' = 0.5$



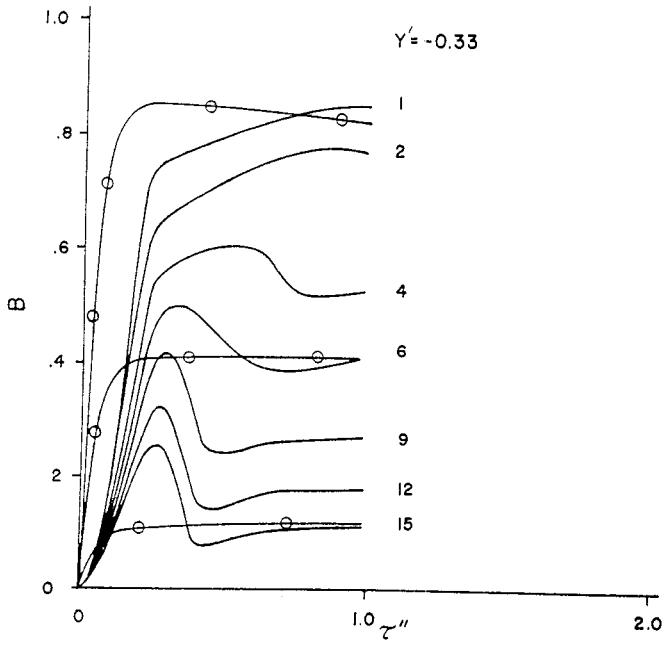
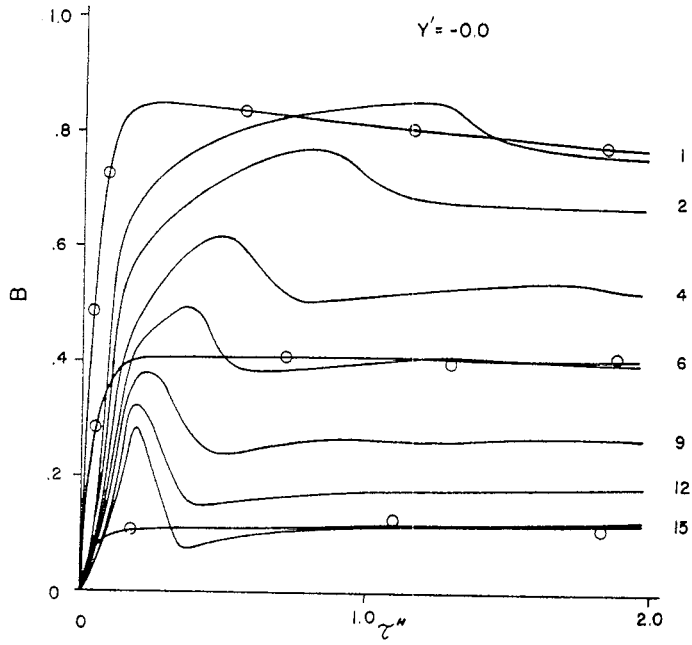
$\gamma' = 0.2$



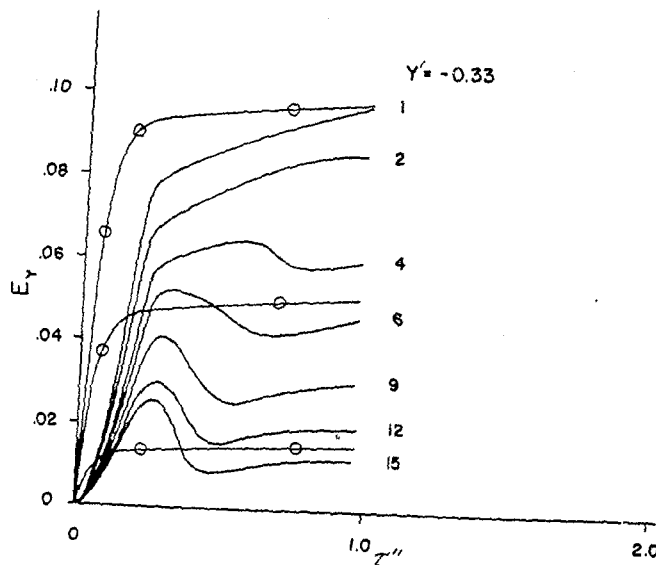
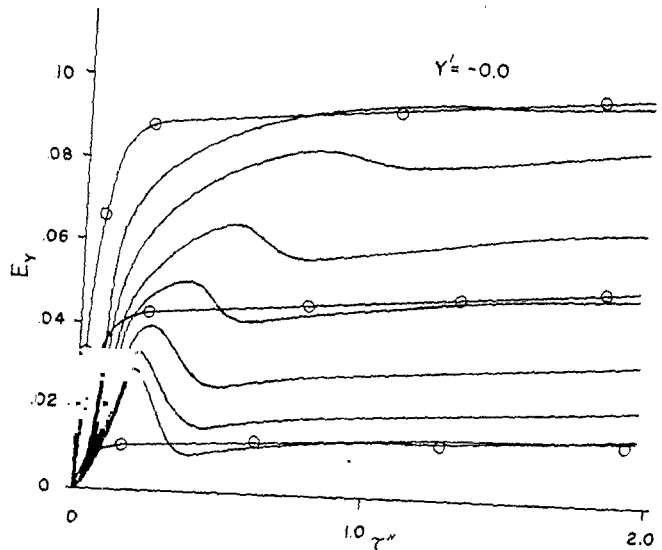
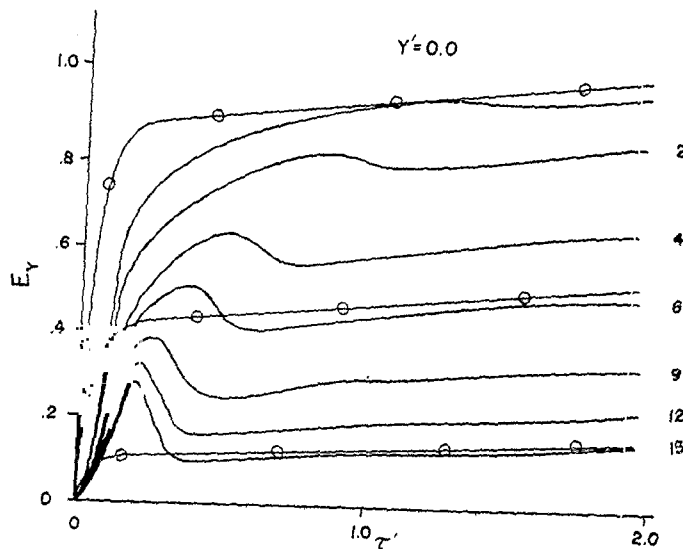
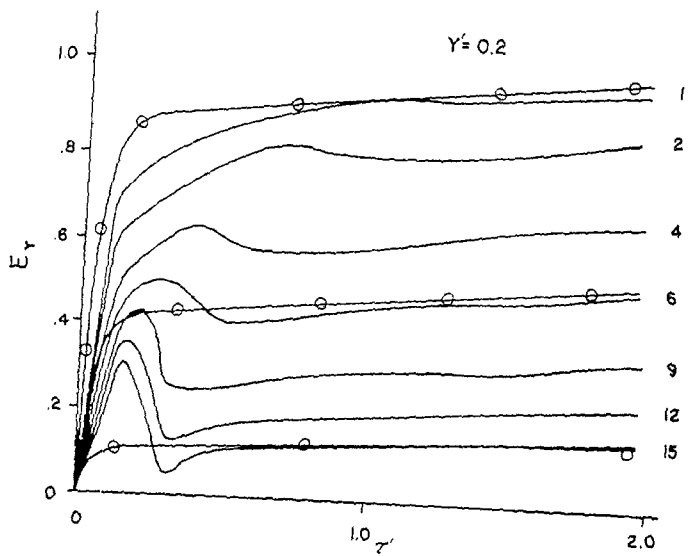
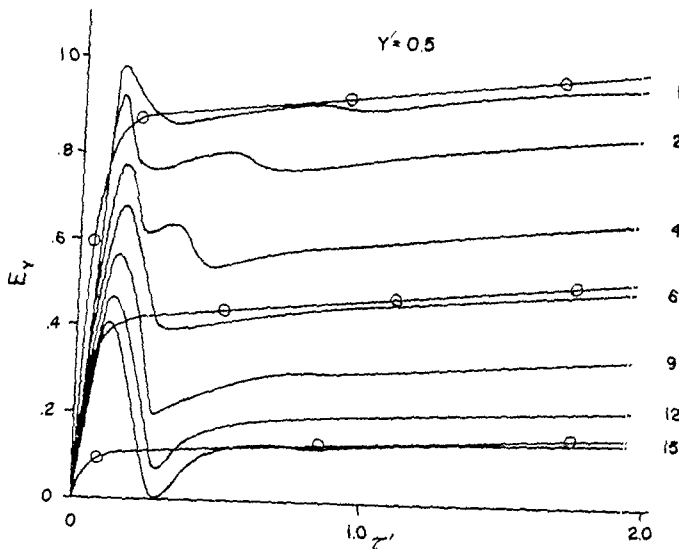
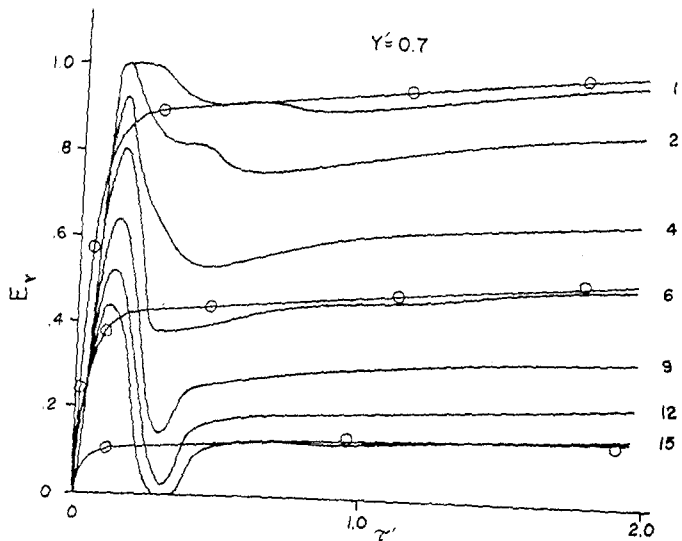
$\gamma' = 0.0$



$\sigma = 0.0001$



$\sigma = 0.0001$



$\sigma = 0.0001$

